SPOT-VGT COLLECTION 3
PRODUCTS USER MANUAL

Authors: Erwin Wolters, Else Swinnen, Carolien Toté, Sindy Sterckx
Version: 1.0
Date:15/06/2016

DOCUMENT CONTROL

Signatures

Authors	Erwin Wolters, Else Swinnen, Carolien Toté, Sindy Sterckx
Reviewers	Dennis Clarijs, Bart Deronde
Approvers	CNES
Issuing authority	VITO

Change record

Release	Date	Updates	Approved by
1.0	15/6/2016	First external version	Bart Deronde, CNES

TABLE OF CONTENTS

LIST OF FIGURES

LIST OF TABLES

LIST OF ACRONYMS

Acronym	Explanation
AATSR	Advanced Along-Track Scanning Radiometer
ACE	Altimeter Corrected Elevations
AOT	Aerosol Optical Thickness
ARPEGE	Action de Recherche Petite Echelle Grande Echelle
AVHRR	Advanced Very High Resolution Radiometer
BELSPO	Belgian Science Policy Office
CESBIO	Centre d'Études Spatiales de la Biosphère
CGP	Ground Control Point
CNES	Centre National d'Études Spatiales
CTIV	Centre de Traitement des Images VEGETATION
DEM	Digital Elevation Model
DWC	Digital Chart of the World
EO	Earth Observation
ERS	European Remote Sensing
FOV	Field of View
FTP	File Transfer Protocol
FWHM	Full Width at Half Maximum
GCM	Global Climate Model
GCP	Ground Control Point
HDF	Hierarchical Data Format
HRVIR	High Resolution Visible
HTTP	Hypertext Transfer Protocol
IPC	Image Processing Centre
MERIS	Medium Resolution Imaging Spectroradiometer
METOP	Meteorological Operational Satellite
MODIS	Moderate Resolution Imaging Spectroradiometer
MVC	Maximum Value Composite
MVC	Maximum Value Compositing
NASA	National Aeronautics and Space Administration
NCSA	National Centre for Supercomputing Applications
NDVI	Normalized Difference Vegetation Index
NEΔR	Noise-Equivalent Delta Radiance
NIR	Near InfraRed
NWP	Numerical Weather Prediction
QIV	Image Quality Centre
RMSE	Root Mean Squared Error
SM	Status Map
SMAC	Simple Model for Atmospheric Correction
SPOT-VGT	Satellite Pour l'Observation de la Terre – Végétation
SWIR	ShortWave InfraRed
TOA	Top of Atmosphere
TOC	Top of Canopy
TOMS	Total Ozone Mapping Spectrometer
WGS84	World Geodetic System - 1984

DOCUMENT OBJECTIVES

This document describes the SPOT-VGT Collection 3 products in terms of data content, format, and changes to the Collection 2 data set. The Collection 3 data set resulted from a reprocessing action that was performed in 2015-2016 after the entire data set had been acquired. In order for the user to understand better the changes to the products, the full description of the Collection 2 data set is provided first. Such comprehensive description was lacking in the past, although most information could be found on the SPOT-VGT website.

The following topics are highlighted:

- Brief overview of the SPOT-VGT instrumental design
- Overview of the original SPOT-VGT product suite (Collection 2)
- Explanation of the various technical and scientific issues that were addressed in the reprocessing
- An overview of the Collection 3 data content and availability, as well as details on the metadata attributes

The document aims at giving a clear overview on the various modifications between SPOT-VGT Collection 2 and Collection 3 data products. The reader is referred to the reference documents below for further information on the various topics related to SPOT-VGT (observations, calibration, validation, etc.).

Reference	Topics
Maisongrande et al., 2004: VEGETATION/SPOT: an operational mission for the Earth monitoring; presentation of new standard products, *Int. J. Remote Sens.,* 25, 9 – 14, DOI: 10.1080/0143116031000115265.	Standard products, improvements, new products
Saint, G., 1994: "VEGETATION" onboard SPOT-4, mission specifications Version 3, *European Commission Joint Research Centre (JRC), Ispra,* 37 pp. Available from www.spot-vegetation.com	Mission specifications, scientific background, instrument design, spatial resolution
Saint, G., 1994: "VEGETATION" onboard SPOT-4, Product Specifications Version 2, *European Commission Joint Research Centre (JRC), Ispra,* 14 pp. Available from www.spot-vegetation.com	Products specifications, input/output data, data format specifications
FAQ list. Available from http://www.spot-vegetation.com/faqnew/index.html	Description of the products and their content
SPOT-VEGETATION User Guide, available from http://www.spot-vegetation.com/pages/documentation.htm	Mission specifications, scientific background, instrument design, products specifications,

1. Introduction to SPOT-VEGETATION mission

The VEGETATION Programme was developed jointly by France, the European Commission, Belgium, Italy, and Sweden. The satellite components of the programme (SPOT-4 and SPOT-5) were launched on 24 March 1998 and 4 May 2002, respectively. The VGT instruments performed measurements from 21 April 1998 until 31 May 2014 and were tailored to monitor land surface variables with a near-daily global coverage at a medium spatial resolution of 1 km.

The VGT mission goals were to provide global data for surface parameter mapping, agricultural, pastoral and forest production and terrestrial biosphere mechanism monitoring and modelling.

Its data have been used for many applications, see below the most important areas, with an example reference selection for further reading:

- **Retrieval of biophysical parameters, such as LAI, fAPAR, albedo:** Pacholczyk et al., 2012, Garrigues et al., 2008, Verger et al., 2009
- **Land cover classification:** Latifovic et al., 2004, Eva et al., 2004, Stibig et al., 2007
- **Agricultural monitoring and food security:** Verdin et al., 2005, Rojas et al., 2005, Savin et al., 2007, Fernandes et al., 2011, Ivits et al., 2011
- **Burnt area detection:** Tansey et al., 2004, Bartalev et al., 2007
- **Forest monitoring:** Mayaux et al., 2005, Zhang et al., 2004
- **Environmental monitoring:** Boschetti et al., 2013

An exhaustive list of publications using SPOT-VGT data can be found at http://www.spot-vegetation.com/.

2. SPOT-VGT instrument characteristics

2.1. VEGETATION instrument design

The VEGETATION instrument, hereafter referred to as VGT, with additions '1' and '2' for the instruments on-board SPOT-4 and SPOT-5, respectively, comprises 4 cameras that observed reflected solar radiation in the following bands: B0 (BLUE, 0.46 µm), B2 (RED, 0.68 µm), B3 (NIR, 0.85 µm), and SWIR (1.66 µm). The cameras covered a field of view (FOV) of 101°, thereby observing a swath of 2,200 km. The nominal pixel resolution was 1.15 km at nadir, increasing to ~1.7 km at the swath extremes.

Each spectral band had its own optics with the associated detector unit in the focal plane. Each detector unit contained:

- an interference filter for spectral selection
- a 1728-detector linear array
- a low-noise amplifier and CCD follower unit
- a SWIR dedicated, closed loop active thermal control concept using a nearby Detection Interface Unit.

Table 1 shows the instrument's main payload and flight characteristics.

Table 1: SPOT-VEGETATION payload and flight characteristics.

Altitude [km]	832
Local overpass time at launch [h]	10:30
Inclination [^{o}]	98.7
Coverage [%]	90 (daily, 100 for latitudes > ±35^{o}), 100 (every 2 days for all latitudes)
Payload mass [kg]	152
Payload dimensions [m^{3}]	0.7 × 1.0 × 1.0
Designed lifetime [yr]	> 5
Instantaneous Geometric Field of View (IGFOV, [km])	1.15

Figure 1 shows the response functions of the four spectral bands for VGT1 and VGT2 and also includes typical vegetation and bare soil spectra. Full Width at Half Maximum (FWHM) spectral ranges and centre wavelengths are summarized in Table 2. The VGT1 response is slightly broader than VGT2 in B0 and B2 at the longer wavelengths, while the VGT1 NIR channel has slightly more response at the shorter wavelengths. The VGT1 SWIR channel is more or less entirely shifted to longer wavelengths, see Table 2 and Table 3 for more details on the spectral ranges, radiometric resolution and radiometric accuracy.

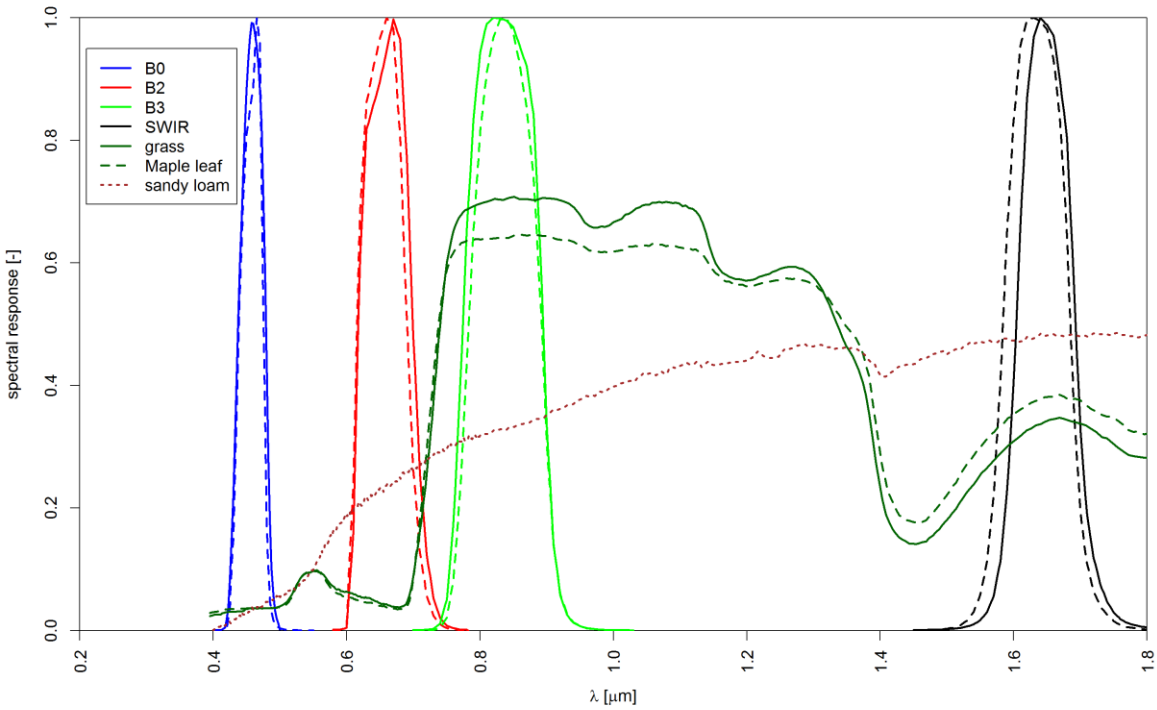

Figure 1: SPOT-VGT spectral response functions for channel B0 (blue), B2 (red), B3 (green), and SWIR (black) for VGT1 (solid line) and VGT2 (dashed line).Typical vegetation spectra for grass (solid dark green line), Maple leaf (dashed dark green line), and bare soil (sandy loam, dotted brown line) are plotted for reference.

Table 2: Spectral ranges (Full Width at Half Maximum, FWHM) and centre wavelengths (in parentheses) for VGT1 and VGT2.

Spectral band	VGT1 [µm]	VGT2 [µm]	Surface reflectance range [-]
BLUE (B0)	0.437 - 0.480 (0.459)	0.439 - 0.476 (0.458)	0.0 – 0.5
RED (B2)	0.615 - 0.700 (0.658)	0.616 - 0.690 (0.653)	0.0 – 0.5
NIR (B3)	0.773 - 0.894 (0.834)	0.783 - 0.892 (0.838)	0.0 – 0.7
SWIR (MIR)	1.603 - 1.695 (1.649)	1.584 - 1.685 (1.635)	0.0 – 0.6

Table 3: Radiometric resolution (NEΔR), intra-image consistency, and radiometric calibration accuracy for all spectral channels.

Radiometric resolution (NEΔR)	8 bits
BLUE	0.003 for the entire spectral range
RED	0.001 up to reflectance of 0.10, linear increase up to 0.003 for reflectance of 0.5
NIR, SWIR	0.003 for the entire spectral range
Intra-image consistency	within an entire image, corresponding to a NEΔR of 0.005 for any reflectance value
Calibration accuracy	Inter-band and multi-temporal: <3% absolute: <5%.

2.2. Geometric characteristics

Table 4 lists the SPOT-VGT geometric characteristics and further provides information on the daily coverage.

Table 4: SPOT-VGT geometric characteristics

Spatial resolution	1.15 km at nadir for both viewing directions	
Field of view	maximum off-nadir observation angle of 50.5° swath width ~2200 km	
Geometric accuracies	***Local distortion***	< 0.3 pixel (<0.35 km at nadir)
	Multispectral registration	0.3 km
	Collocation with HRVIR	0.3 km for simultaneous acquisitions
	Multi-temporal registration	0.5 km
	Location accuracy	1000 m
Spatial coverage	About 90% of the equatorial areas imaged daily, the remaining 10% the next day. Latitudes poleward of ~35° observed at least once per day.	

3. Product overview

The various SPOT-VGT Collections comprise the following products:

- FreeP (Level 2 TOA data)
- S1 products
- S10 NDVI - continental extracts
- S10 Radiometric – continental extracts

Below a short description per product is given, users are referred to Section 7 for a more exhaustive description per product.

3.1. VGT-P products

VGT-P products comprise Top-of-Atmosphere (TOA) reflectance observations in the original segments over land. The data are adapted for scientific applications requiring highly accurate physical measurements. The data are corrected for system errors (error registration of the different channels, calibration of all detectors along the line-array detectors per spectral band, etc.) and projected to Plate Carrée. The pixel digital count (DN) is the ground area's apparent reflectance as seen at Top of Atmosphere (TOA). Auxiliary atmospheric data (on water vapour, ozone, and aerosols) supplied with the products allow users to process the original reflectance values using their own algorithms. Please note that these auxiliary data are not the actual ones, but a monthly climatology. The image products cover all or part of a VGT segment. Figure 2 shows an example of a VGT2 P segment.

Figure 2: VGT2 segment (B2 channel) of 25 January 2014 over East Africa and the Middle-East.

3.2. VGT-S products

3.2.1. VGT S1 products

VGT-S1 products (daily synthesis) are composed of the 'best available' surface reflectance measurements of all segments received during one day for nearly the entire Earth's surface. This is done for each image covering the same geographical area. High-latitude areas are more frequently observed and thus have more overlapping parts, so for these areas the best observation is selected from multiple observations. The S1 product provides data from all spectral bands (B0, B2, B3, and SWIR), the NDVI, and auxiliary data on image acquisition parameters. Figure 3 shows an example NDVI image from one day of VGT2 observations.

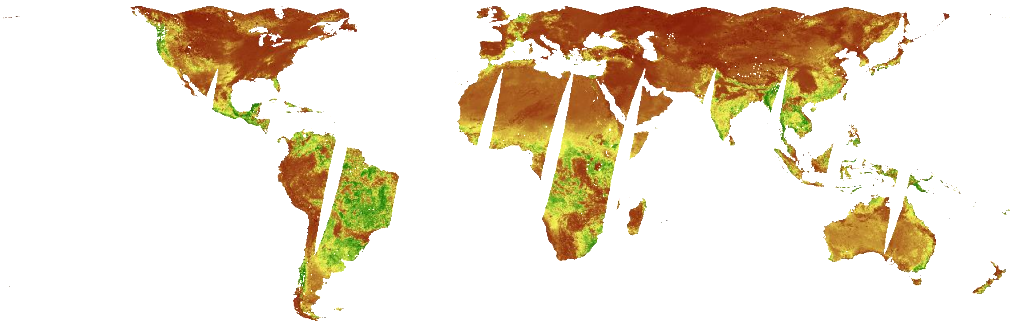

Figure 3: NDVI image composed of VGT2 S1 observations on 5 January 2014. The colour scale runs from dark brown (low NDVI) to green (high NDVI).

3.2.2. VGT S10 products

The VGT-S10 are global, 10-day composite images composed from the 'best available' SPOT-VGT observations over a 'dekad' (i.e., from day 1 – 10, 11 – 20, and 21 – end of the month). The products provide data from all spectral bands (SWIR, NIR, RED, BLUE), the NDVI, and auxiliary data on image acquisition parameters.

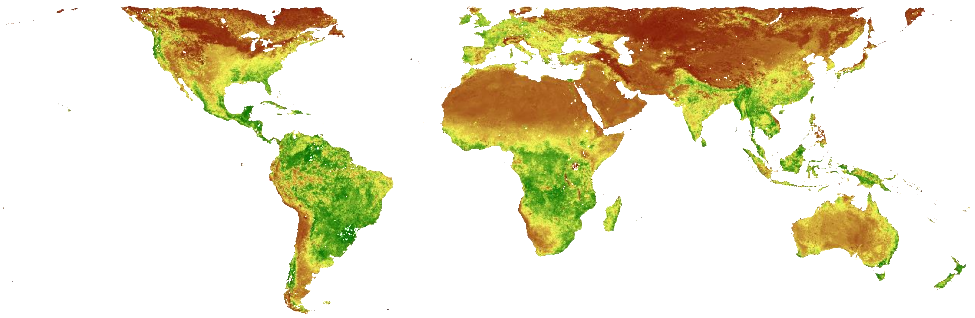

Figure 4: NDVI image composed of VGT2 observations for 11 – 20 January 2014. The colour scale is similar as in Figure 3.

3.3. Data availability

All SPOT-VGT data are available in Hierarchical Data Format version 4 (HDF4) format from the VITO Earth Observation portal: http://www.vito-eodata.be. More information on the data access and registration process can be found in Section 7.

The Hierarchical Data Format, or HDF4, is a multi-object file format for sharing scientific data in a distributed environment. HDF was created at the National Centre for Supercomputing Applications (NCSA) to serve the needs of diverse groups of scientists working on projects in many fields. HDF was designed to address many requirements for storing scientific data, including:

- Support for data and metadata commonly used by scientists.
- Efficient storage of and access to large data sets.
- Platform independence.
- Extensibility for future enhancements and compatibility with other standard data formats.

HDF files are 'self-describing', which means that for each data object there is information about the data type, the data amount, its dimensions, and its location in the file. Further, HDF supports incorporating multiple datatypes within a single file.

4. Collection 2 processing

4.1. Introduction

The VGT image quality relies not only on the satellite and the instrument, but also on the ground segment and in particular the image processing. All data acquired by the VGT instruments were downloaded at the Kiruna receiving station (Sweden) and transferred to the Central Processing Facility (Centre de Traitement des Images VEGETATION, CTIV) for processing and archiving.

Figure 5 shows the main processing steps used in the VGT Image Processing Centre. The main steps of the processing from raw data received from Kiruna (Level1A) to synthesis data for end-users (Level 3) comprise the following:

- Geometric correction
- Radiometric correction
- Pixel quality labelling
- Atmospheric correction
- Synthesis composition

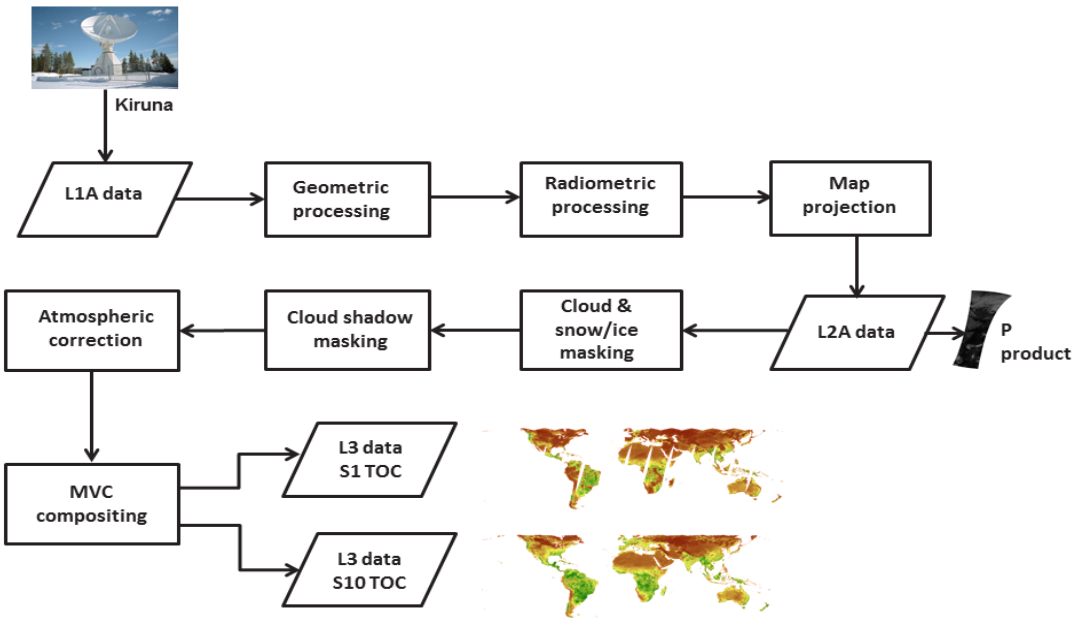

Figure 5: The SPOT-VGT data processing scheme.

The separate processing steps are described in the following subsections.

4.2. Geometric correction

As the main use of VGT data was in monitoring the vegetation evolution over a large time period, the need for a very accurate multi-temporal registration was translated in the following requirements:

- absolute location accuracy less than 1 km
- multi-temporal registration better than 500 m for 95% of the points (i.e., at 2 σ in case of a Gaussian distribution), with an objective of 300 m
- multi-spectral registration better than 300 m

Because the geometric calibration was done differently for VGT1 and VGT2, the processing steps will be explained for each of the instruments separately.

Initial pre-flight assessment of the VGT1 geolocation accuracy revealed an Root Mean Square Error (RMSE) of ~1 km and initial post-launch geometrical performance was 800 m. In order to become compliant with the user requirements, it was decided to generate a Ground Control Points (GCPs) database to improve the geolocation accuracy at the start of every orbit. SPOT High Resolution Visible (HRVIR) instrument chip sets with an estimated geolocation accuracy of ~100 m, were used to increment the GCP database, which finally consisted of 3650 GCPs (Sylvander et al., 2003). Figure 6 shows the global distribution of the GCP database.

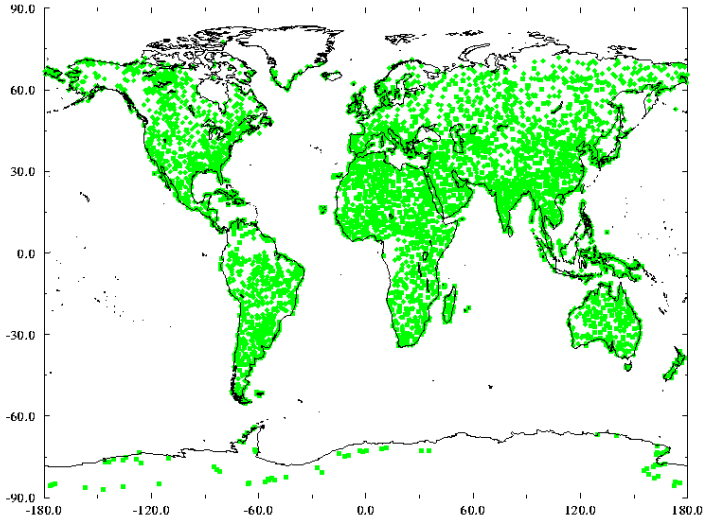

Figure 6: Global distribution of the GCP database (from: Sylvander et al., 2003).

Using the GCP database, the geometrical performance significantly improved, with a decrease of the absolute location RMS error from 725 m before March 1999 to 300 m in 2000 and further improving to 190 m afterwards. Likewise, the 95% absolute location error improved from 1380 m before March 1999 to 375 m after 2000. The multi-temporal registration error decreased from 885 m RMSE (March 1999) to 220 m.

The VGT2 geolocation requirements were similar to those of VGT1. However, as the SPOT-5 satellite carried a star tracker on-board, which provided an accurate estimate of the satellite's attitude, no GCP database was required for VGT2. The final geolocation RMS and 95% errors for VGT1 and VGT2 are summarised in Table 5.

Table 5: RMS and 95% absolute location errors for VGT1 and VGT2.

	Absolute Location Error		Multi-Temporal registration	
Instrument	**RMS**	**MAX(95%)**	**RMS**	**MAX(95%)**
VGT1	190 m	375 m	220 m	450 m
VGT2	170 m	345 m	155 m	320 m

4.3. Radiometric correction

The user requirements with respect to the SPOT-VGT radiometric calibration were as follows (Table 6).

Table 6: SPOT-VGT calibration requirements (from: Henry and Meygret, 2001).

	VGT calibration requirement [%]
Absolute calibration accuracy	5
Multi-temporal calibration accuracy	3
Interband accuracy	3
HRVIR/VGT intercalibration accuracy	3

The operational calibration monitoring was initially performed using on-board calibration lamps (see Henry and Meygret, 2001, for more details), but at a later stage vicarious calibration was necessary due to degradation of the on-board lamps. This vicarious calibration was carried out monthly over stable desert sites and was validated using Rayleigh calibration [see e.g. Vermote and Kaufman (1995), Vermote et al., (1992) for more details on the methodology] and for the inter-band calibration deep convective clouds [e.g. Doelling et al., (2013), Sterckx et al., (2013), Sohn et al. (2009)] and sun-glint areas [see e.g. Hagolle et al. (2004) and Vermote and Kaufman (1995)]. The results for VGT1 and VGT2 are summarised below.

For VGT1, an extensive calibration was carried out by Henry and Meygret (2001). It consisted among others of available on-board calibration, vicarious calibration over desert sites, and calibration over deep convective clouds. Using these methods, it was demonstrated that the radiometric user requirements were met.

For VGT2, several vicarious calibration efforts over desert sites were performed. In general, the VGT2 absolute radiometric calibration was found in good agreement with other sensors, such as

MODIS, MERIS, and AATSR. Reported inter-calibration differences are within ±4% [see e.g. Lachérade et al. (2013), Bouvet (2014)].

4.3.1. TOA reflectance computation

The top of atmosphere (TOA) reflectance computation is performed in several steps. To compensate for the differences between each detector of the viewing line, the normalization takes into account parameters computed at the Image Quality Centre (QIV) at CNES, which gives for every detector its characteristics. In the instruments, especially in the SWIR, some detectors were blind because they were located between two detector chips, while others were declared defective after being hit by protons. The observations given by these detectors were ignored and replaced by interpolated observations from the neighbouring detectors. Subsequently, the TOA radiance was computed from the normalized digital count, using the absolute calibration parameters from QIV. Finally, the TOA reflectance was computed, taking into account the solar irradiance model, the solar angles, and sun-earth distance. The TOA NDVI was also calculated for temporary use in the synthesis processing.

Note that the Sun-Earth distance modelling was not performed accurately, which was communicated to the users on 12 June 2012 (see http://www.spot-vegetation.com/pages/newsupdates.html). More information on this issue can be found in section 5.1.

4.4. Pixel quality labelling

4.4.1. Snow/ice and cloud detection

4.4.1.1. Snow/ice detection

In the initial version of the processing chain (version V1, which was operated until 11 May 2001), snow/ice was identified according to the following rules (see Table 7):

Table 7: Threshold values for the SPOT-VGT snow/ice detection until 1999.

start of operational use	threshold values
05/12/1997	B0 > 0.95; B2 > 0.46; B3 > 0.47; SWIR > 0.98
12/01/1999	B0 > 0.337; B2 > 0.297; B3 > 0.2605; SWIR > 0.164

For the snow/ice detection in Collection 2, a number of threshold tests were applied:

$$T_1 = R_{B0}$$

$$T_2 = R_{SWIR}$$

$$T_3 = \frac{R_{B0} - R_{B3}}{R_{B0} + R_{B3}}$$

$$T_4 = \frac{R_{B0} - R_{SWIR}}{R_{B0} + R_{SWIR}}$$

$$T_5 = \frac{R_{B0} + R_{B2}}{2} - R_{SWIR}$$

The decision tree for the V2 snow/ice detection is presented in **Figure 7**.

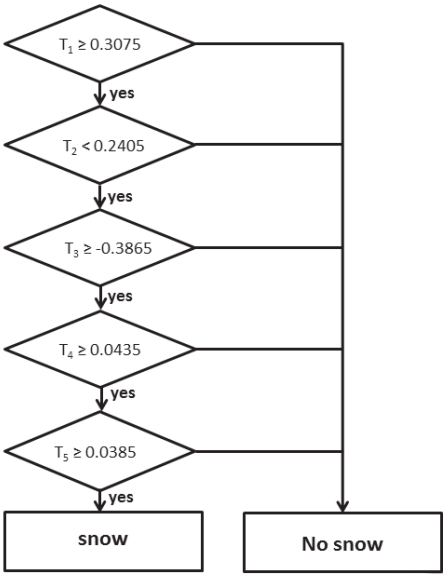

Figure 7: Snow/ice detection decision tree for Collection 2.

4.4.1.2. Cloud detection

Version 1 (V1) of the cloud detection method consisted of a number of threshold tests applied to all spectral channels, see Table 8 for the threshold values.

Table 8: Cloud detection threshold values applied until 1999.

Date of operation	
26/11/1998	B0 > 0.29; B2 > 0.50; B3 > 0.50; SWIR > 0.50
01/01/1999	B0> 0.1975; B2 > 0.147; B3 > 0.243; SWIR > 0.2245
08/02/1999	B0 > 0.337; B2 > 0.2745; B3 > 0.2605; SWIR > 0.164

For cloud detection version 2 (V2, from 12 May 2001 onwards), an algorithm proposed by Lissens et al. (2000) was implemented. The TOA reflectances were evaluated as follows:

A pixel is declared **'clear'** if:
$R_{B0} < 0.2465$ OR $R_{SWIR} < 0.09$

A pixel is declared **'cloudy'** if:
$R_{B0} \geq 0.36$ AND $R_{SWIR} \geq 0.72$

A pixel is declared '**uncertain'** if:
It is not declared clear or cloudy by the previous two rules.

4.4.2. Cloud shadow detection

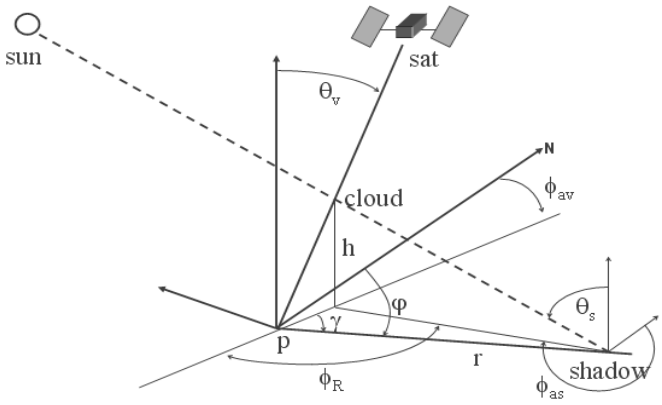

Figure 8: Depiction of solar, satellite, cloud, and cloud shadow geometries (image from Lissens et al., 2000).

Cloud shadow detection is of importance to land surface research, as the dark areas casted at the Earth surface can lead to erroneous vegetation parameter retrievals. The methodology to screen for cloud shadows is a hybrid between the radiometric approach (see e.g. Zhu and Woodcock, 2012 and Ackerman et al., 2010) and a geometric approach (see Simpson et al., 2000).

The geometric part of the cloud shadow detection algorithm is presented in Lissens et al. (2000) . A cloud pixel is located at position *p*, with the actual cloud being at height *h* from the tangential plane, i.e., the intersection of the sun beam and the line of sight from the satellite to the cloud pixel. The cloud shadow can then be found as the intersection of the sun beam and the tangential plane at the centre. Solar zenith and azimuth angles are assumed to be equal in the cloud and cloud shadow pixels. It follows from Figure 8 that angle φ equals the sum of Υ and the viewing azimuth angle ϕ_{av}. When φ and the distance between the cloud and associated cloud shadow pixel, *r*, are known, their position can be calculated using geometry.

Cloud heights are estimated using the gradient in NIR reflectance along the projected path from a cloud to its shadow in the image (
Figure 9). In case of a cloud shadow, the NIR reflectance will decrease towards a minimum from cloud to shadow edge. If this change is above a threshold of 20%, a shadow edge is detected. From the locations of the cloud and shadow edge, the cloud height can subsequently be calculated.

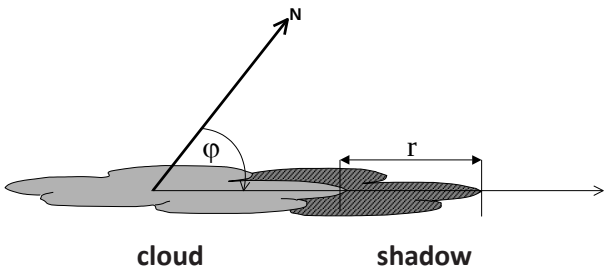

Figure 9: Concept of NIR reflectance tracing away from cloud edge to shadow edge (image from Lissens et al., 2000).

4.5. Atmospheric correction

The atmospheric correction is based on the use of the Simplified Model for Atmospheric Correction [SMAC, Rahman et Dedieu (1994], which is a simplified inversion of the 6S method (Tanré et al., 1990). The SMAC parameters were derived for the VGT1 and VGT2 spectral bands (Berthelot and Dedieu, 1997). The auxiliary data used as SMAC input are water vapour, ozone, tropospheric aerosol and a digital elevation model.

4.5.1. Water vapour

Until 7 April 2008, the 6-hourly gridded total column water vapour from the global short term ARPEGE Numerical Weather Prediction (NWP) model of Metéo-France was used in the atmospheric correction. The model grid resolution was 1.5° × 1.5° (~170 × 170 km^2). Geometrical interpolation was performed to obtain 8/112° × 8/112° (~8 × 8 km^2) cells and temporal interpolation was performed between the two nearest NWP model outputs, taking into account the SPOT-VEGETATION observation time.

Since 8 April 2008, Water Vapour data are obtained from MeteoServices. These data consists essentially of the ECMWF total column water vapour 6-hourly data, but are gridded at a 0.25° × 0.25° resolution.

4.5.2. Ozone

Ozone information is obtained from an ozone climatology from the Centre d'Études Spatiales de la Biosphère (CESBIO), which was composed from 11 years of TOMS data. One global set is available at 0.25° × 0.25° resolution for each month, with the data being representative for day 15. To calculate corrections for a certain day, the preceding and consecutive monthly climatology file is obtained and interpolated linearly.

4.5.3. Tropospheric aerosol

Until 10 May 2001, the SPOT-VGT images were corrected using a simple static aerosol model obtained from CESBIO, in which the Aerosol Optical Thickness (AOT) was solely dependent on the latitude of observation:

$$\tau_{550} = 0.2 \cdot (\cos(latitude) - 0.25) \cdot \sin\left(latitude + \frac{\pi}{2} \right)^3 + 0.05 \text{ (Eq. 1)},$$

with τ referring to the AOT. In order to improve the atmospheric correction, an AOT retrieval method using the VGT B0 and SWIR channels was used from 11 May 2001 onwards.

The aerosol optical thickness (AOT) retrieval method is based on a method of Maisongrande et al. (2001), which utilises a relation between the TOA NDVI and the observed SWIR reflectance. The AOT retrieval is performed as follows:

1. For each spectral channel, an initial atmospheric correction is calculated taking only gaseous absorption by water vapour and ozone and molecular scattering into account. This initial atmospheric correction is only applied to pixels that are labeled as 'clear' by the preceeding cloud screening algorithm and further not labeled as 'snow/ice'. The obtained reflectances are herafter referred to as $R_{TOC,mol}$.
2. From the NIR_{TOA} and RED_{TOA} reflectances, the $NDVI_{TOA}$ is calculated.
3. From the $NDVI_{TOA}$, $Ratio = R_{SWIR,TOC} / R_{BLUE,TOC}$ is derived, using the relation $Ratio = 1.305 * \exp(3.225 * NDVI_{TOA})$. This also gives information on $R_{SWIR,\ TOC}$, because in the SWIR spectral range the atmospheric scattering is negligible and thus $R_{SWIR,TOC} = R_{SWIR,mol}$.
4. $R_{BLUE,TOC}$ is calculated from $Ratio$ and $R_{SWIR,TOC}$ obtained in the previous step.
5. For aerosol optical thickness values of 0.05, 0.15, 0.30, and 0.50, the difference between reflectance from SMAC with full atmospheric correction (gaseous absorption + molecular scattering + aerosol contribution) and $R_{BLUE,TOC}$ obtained in step 4 is calculated. The retrieved aerosol optical thickness is one of the four AOT values above for which this difference is minimal.
6. $NDVI_{TOC,mol}$ and $R_{SWIR,TOC,mol}$, are assessed against thresholds of > 0.2 and < 0.4, respectively. For pixels fulfilling these criteria, the aerosol optical thickness follows from the retrieved value in step 5. For pixels outside these criteria, the aerosol optical thickness is empirically estimated based on the latitudinal function of Eq. 1.

Subsequently, the obtained AOT representative at 0.55 µm was converted to corresponding B0, B2, B3, and SWIR values using a continental aerosol model and full atmospheric corrections to all TOA reflectances were performed.

It is noted that the AOT retrieval procedure was only applied to pixels complying to a number of criteria, i.e. no snow, NDVI above an empirical threshold (NDVI > 0.2) and the SWIR reflectance below an empirical threshold (SWIR < 0.4). If these conditions were not met (e.g. over deserts), then the original fixed latitudinal aerosol "climatology" of Eq. 1 was used. Note that due to computational restrictions the aerosol optical thickness was only retrieved with the above method for every $8^{th} \times 8^{th}$ pixel.

4.5.4. Digital Elevation Model (DEM)

The Altimeter Corrected Elevations (ACE) Digital Elevation Model (DEM), at 8/112^{o} resolution was used to estimate air pressure. ACE DEM was composed from Radar Altimeter observations on-board the European Remote Sensing Satellite 1 (ERS-1). See Berry et al. (2000) for more details.

4.6. Compositing procedure

The purpose of compositing is to optimally combine multiple observations over a given time interval into a single and cloud-free synthesis image. The operation starts from atmospherically corrected segment data (except for the TOA NDVI that is calculated for pixel compositing selection) and takes into account the variation in residual clouds and the sensor viewing and solar angle conditions. The compositing steps minimize the cloud effect and angular variations and maximize global coverage. This allows for depicting spatial and temporal variations in vegetation.
Another reason to perform compositing is that daily descending SPOT-VGT orbits did not completely overlap, especially near the equator. To obtain global coverage, at least two orbiting days were needed.

The compositing rules to arrive at 10-day syntheses are as follows:

- Observations covered by all spectral bands are preferred over observations covered by only a few spectral bands.
- Observations with a good pixel quality indicator for the B0, B2, and B3 bands are preferred over observations of less quality.
- Cloud-free observations are preferred over ice/snow observations, which in turn are preferred over cloud observations.
- In case two or more observations are still of equal quality, the observation yielding the maximum TOA NDVI value is preferred.

Sea or lake is determined from a sea/land static indicator, derived from the “Digital Chart of the World” [DCW, Danko (1992)], where land areas have been expanded by 5 km to cover the inaccuracy of the DCW, to cover cases of tides or growing river deltas, and not to alter real shore pixels by interpolating them with null data.

5. Collection 3 change summary

The decision on reprocessing the entire SPOT-VGT archive was taken to further improve the data quality to the latest scientific and technical insights and to correct for known errors. The major reprocessing actions taken are listed below.

5.1. Earth-Sun distance error correction

As the Earth orbits the Sun in an elliptic orbit, the Sun – Earth distance differs between 147.1 million km (at 3 July) and 152.1 million km (at 3 January). As a result, the amount of solar irradiance that reaches the Top of Atmosphere (TOA) differs accordingly. The difference in solar irradiance between January and July is ~7%.

During the preparation of the PROBA-V ground segment processing, a review of the VGT processing was performed. This revealed that the date used to calculate the Sun-Earth distance in the processing chain was fixed. In order to avoid disrupting operational applications based on multi-annual VGT data analysis, it was decided not to change the processing chain at that time, but to postpone its correction until after the latest VGT acquisition (see also communication to users on 12 June 2012 http://www.spot-vegetation.com/pages/newsupdates.html).

The erroneous Sun-Earth distance modelling directly impacts the VGT-P products (TOA), and for these products, the correction factors were supplied to the users. For the synthesis products, the correction factor could not be applied directly because the ratio between TOA and TOC reflectance is not the same for the different bands and mainly depends on the actual atmospheric state.
In Collection 3 VGT, the Sun-Earth distance modelling is correctly implemented.

Figure 10 shows the relative difference between Collection 2 and Collection 3 TOA reflectances. The correction results in a seasonal reflectance change, with the largest change (7%) on 1 July and no change on 1 January (see Figure 10). This correction is thus identical from one year to the next and affects both instruments and all spectral bands in the same way.

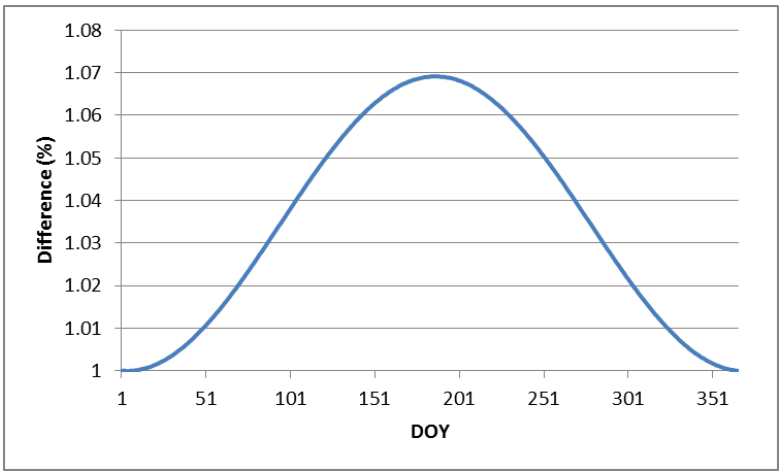

Figure 10: Difference (in %) between TOA reflectance values in Collection 2 and Collection 3 related to correction of Sun-Earth distance modelling.

5.2. Cloud and snow/ice detection modifications

In the Collection 2 VGT archive, the cloud and snow/ice detection changed from V1 to V2 on 11 May 2001. This change resulted in a larger amount of detected clouds. Still, omission errors were present in the detection. In the Collection 3 dataset, this was further improved by adding a number of rules to the existing V2 cloud and snow/ice detection schemes in the processing chain.
Additional rules were derived from Quesney (2008) and Berthelot (2004) for cloud and snow/ice detection, respectively. These are referred to as CLOUD V3 and SNOW/ICE V3, whereas the C2 algorithms are both V2.

The order of the detection is the following:

- First, both the V2 methods are applied (CLOUD and SNOW/ICE). Outputs are a cloud_V2 and snow_V2 flag. After this step, the cloud shadow detection is performed.
- Next, the SNOW/ICE V3 detection is done, which creates a temporary output snow_V3 flag, as well as a flag for band saturation.
- Then, the V3 cloud detection is added, which creates a temporary output cloud_V3 flag. No check is done in the following cases:
    - If CLOUD V2 returned a “cloud” or “uncertain” flag, and
    - If SNOW/ICE V3 resulted in a snow_V3 flag.
- If a temporary cloud flag exists, it is first applied. Only after, a temporary snow flag is applied. Then, the cloud shadow is applied for the cloud_V3 flags.

The result is that more clouds are detected. Visual checks have shown that there is a large improvement. A full validation of the cloud and snow/ice masking is planned.

5.3. High-frequency calibration correction

Each VGT1 and VGT2 detector was calibrated during commissioning. However, over time, these detectors have evolved differently, while no calibration corrections were applied. This eventually resulted in stripes in the images. An investigation on the temporal evolution of the high-frequency calibration factors was carried out by the Centre National d'Études Spatiales (CNES). Using VGT1 and VGT2 images over the Antarctic Dome C station, it appeared that the stripe effects were well visible throughout the entire VGT1 and VGT2 era in the P segments.

Subsequently, new high-frequency calibration factors were calculated to mitigate the striping effects. More information on the methodology and derived new calibration coefficients can be found in Quang et al. (2015).

5.4. Calibration and equalisation over the Field of View (FOV)

In the reprocessing, both the absolute calibration and the equalization factors over the field-of-view (FOV) were revised. The aim of the adjusted absolute calibration is to better characterize the conversion of digital counts measured by the instruments into reflectance values and in particular to better model how the instruments' sensitivity evolved over their orbital lifetime. The improved relative in-field calibration corrects for the so-called 'smile' effect. The Top-of-Atmosphere (TOA) radiance R_{TOA} is related to both factors and both have to be taken into account simultaneously:

$$R_{TOA,i} \sim \frac{DN_i}{A_i . g_i}$$

with
- $\boldsymbol{A_i}$ the absolute calibration which is a function of time
- $\boldsymbol{g_i}$ the equalization, which varies over the field of view and over time
- $\boldsymbol{DN_i}$ the digital number
- $\boldsymbol{i}$ the spectral band

In addition, an adjustment was done to remove the high-frequency noise in the SWIR channel.

5.4.1. Absolute calibration VGT1

Figure 11 shows the evolution of the VGT1 absolute calibration coefficients over time and their difference expressed in percentage relative to the old set of coefficients. A positive difference indicates that the new calibration coefficient is higher than the one of Collection 2 (C2) and that the TOA radiance is lower, given that the equalization is unchanged.

For all bands, the differences in calibration coefficients between C2 and C3 are very limited (<1%). The largest differences in absolute calibration coefficients are observed for the first year (1998 till mid 1999). Afterwards, a gradual decrease in calibration coefficients is observed for the BLUE, RED

and NIR bands. For the SWIR band, a slight increase in the absolute calibration coefficient is seen. The absolute calibration of the RED channel shows the smallest differences between Collection 3 and Collection 2.

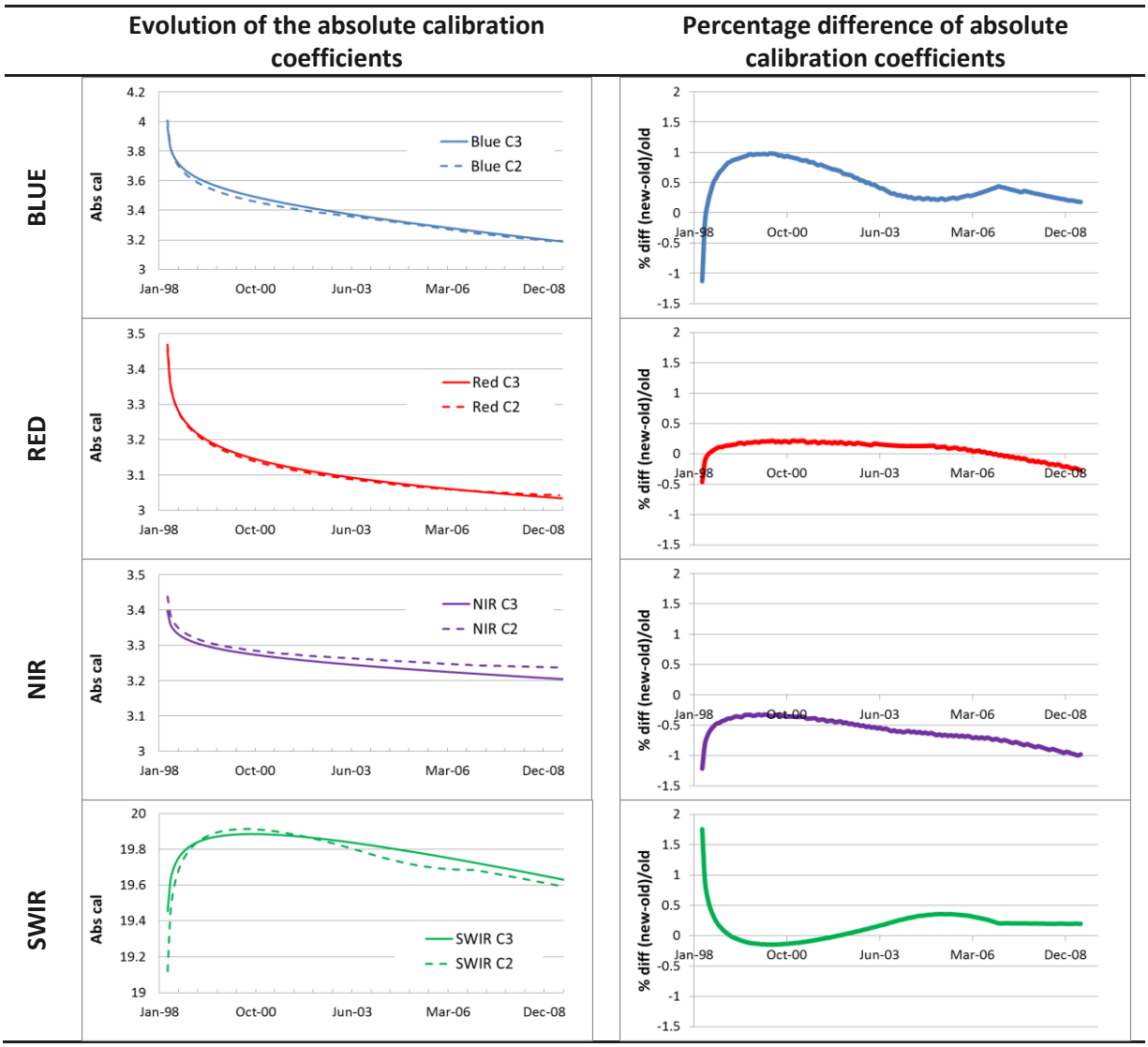

Figure 11 Left: Evolution of the absolute calibration coefficients of VGT1, Right: Difference between the new and old relative to the old absolute calibration coefficients

The change in equalization over the FOV varies only slightly over time. Those for one particular date are shown in Figure 12. If the percentage difference is positive, the equalization coefficient is higher than in C2, resulting in lower TOA reflectances with unchanged absolute calibration coefficients. Overall, the change in the calibration coefficients of VGT1 is limited.

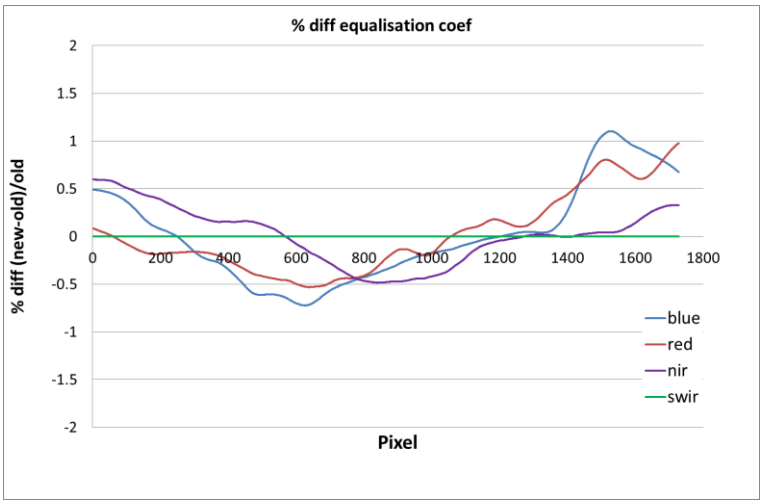

Figure 12: Relative difference [%] between the C3 and the C2 equalization coefficients relative to the C2 equalization coefficients for VGT1.

5.4.2. Absolute calibration VGT2

Figure 13 shows the evolution of the VGT2 absolute calibration coefficients over time and their difference expressed in percentage relative to the old set of coefficients. A positive difference indicates that the new calibration coefficients are higher than the old ones and that the TOA radiance is lower, given that the equalization is unchanged.

Overall, the changes in calibration are larger for VGT2 than for VGT1. For BLUE, the difference between C2 and C3 calibration coefficients gradually increases, resulting in a reduction of TOA radiance. For the RED band, the difference varies over the years: from summer 2003 till approx. April 2004 the C3 calibration coefficient is lower (resulting in higher TOA radiance), while for 2006-2007 the C3 calibration coefficient is higher. Only marginal differences are observed since 2009. For NIR, the difference varies over the years, but overall the magnitude of the difference is limited. The change in calibration between C2 and C3 is almost negligible for the SWIR channel.

	Evolution of the absolute calibration coefficients VGT2	Percentage difference of absolute calibration coefficients VGT2
BLUE	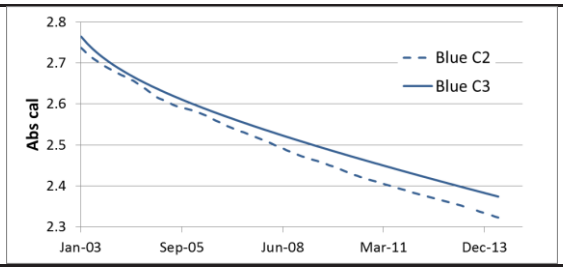	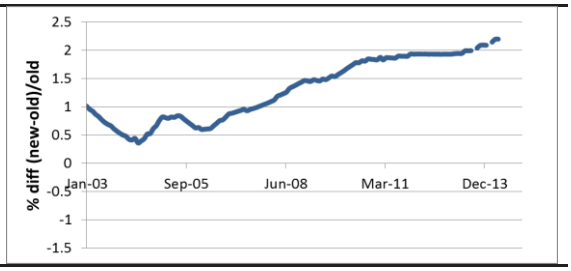

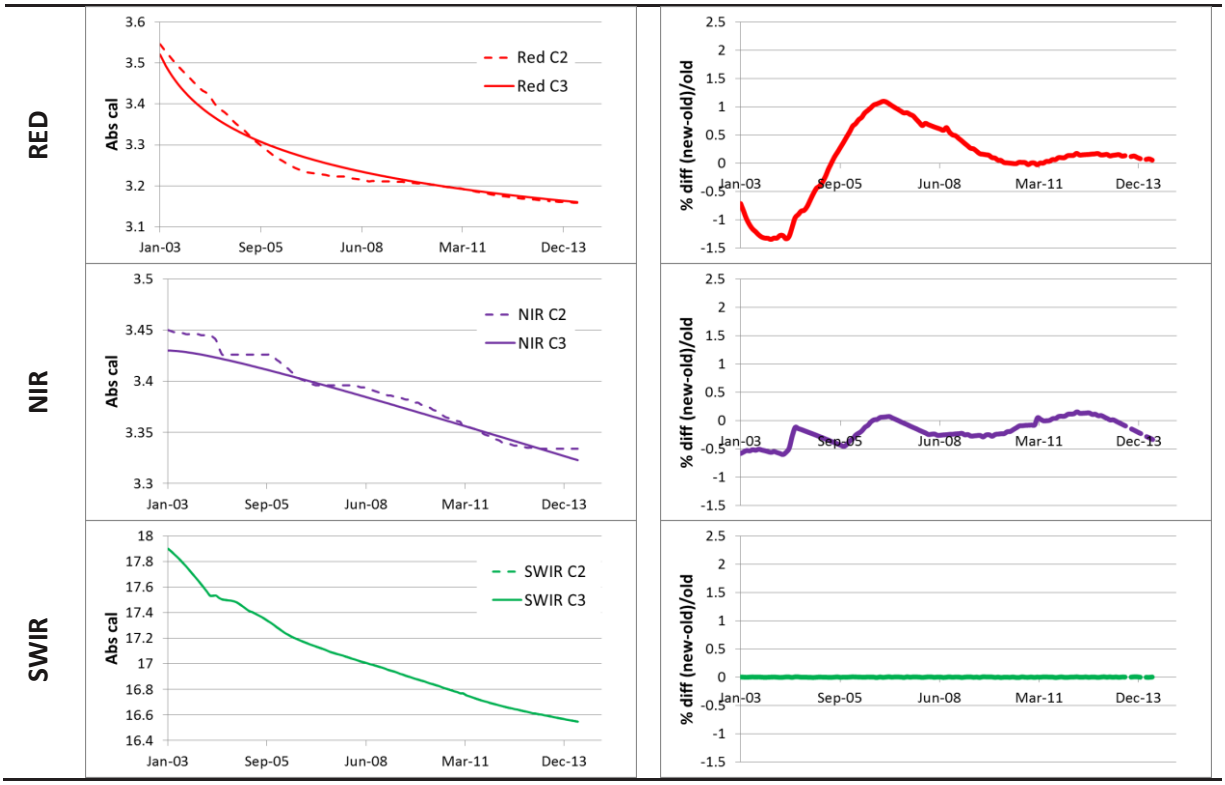

Figure 13 Left: evolution of the absolute calibration coefficients of VGT2, Right: Difference between the new and old relative to the old absolute calibration coefficients.

The change in the equalization over the field of view is varying only slightly over time. Those for one date are shown in Figure 14. If the percentage difference is positive, the equalization coefficient is higher than in C2, resulting in lower TOA reflectances with unchanged absolute calibration coefficients.

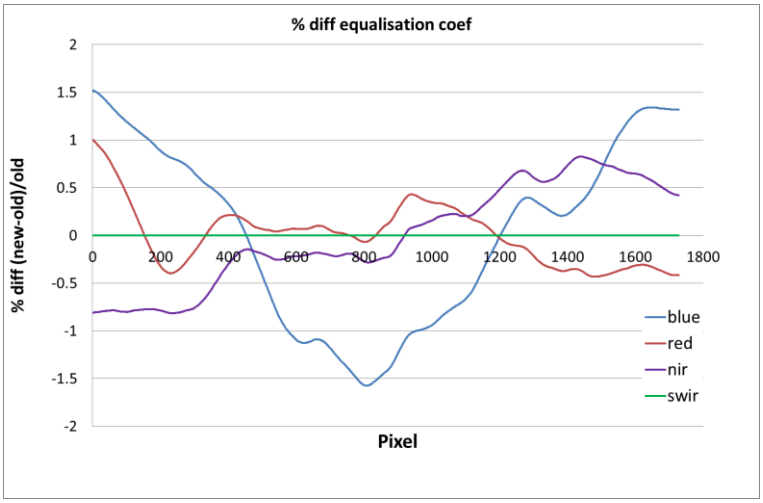

Figure 14: Relative difference [%] between the new and the old equalization coefficients relative to the old ones for VGT2 (for a specific date).

For SWIR, there is no change in the re-processed archive, only in the high-frequency calibration. The smile effect present in the BLUE band is corrected for. Overall, the changes in equalization are larger for VGT2 than for VGT1.
Note that since Collection 2, VGT1 and VGT2 are intercalibrated.

5.5. Aerosol optical thickness retrieval modification

Table 9 shows the two AOT retrieval versions that were used in the various SPOT-VGT Collections. From 11 May 2001 onwards, the AOT retrieval for the atmospheric correction step has been estimated from the B0 and SWIR band, as described previously in Section 4.5.3 and which was introduced and described by Maisongrande et al. (2001, 2004).

Table 9: AOT retrieval methods used in the SPOT-VGT Collections

From	To	Algorithm applied
April 1998	10 May 2001	AOT defined by a time-invariant function of latitude
11 May 2001	31 May 2014	AOT is estimated from the B0 and SWIR spectral bands and the NDVI through an optimization process. (Maisongrande et al., 2001, 2004)

6. Quality assessment

The Collection 3 VGT data set has been validated at different levels:

- Evaluation of the different changes in the processing
- Comparison of the data set against the Collection 2 data set
- Comparison of the Collection 3 data set against two reference time series (METOP-AVHRR and Terra-MODIS)

The full details of the validation can be found in Toté et al. (2016). A brief summary of the comparison between Collection 2 and 3 is given below.

6.1. Comparison between Collection 2 and Collection 3

The differences between the Collection 2 and 3 datasets were assessed separately for VGT1 and VGT2 by comparing all spectral band reflectances and NDVI on subsampled data. More details on data selection and masking can be found in Toté et al. (2016). Analyses were performed for April 1998 – January 2003 and February 2003 – May 2014 for VGT1 and VGT2, respectively.

The following research questions were addressed:

- What is the difference in data completeness between Collection 2 and Collection 3, in particular with respect to the Status Map?
- What are the differences between Collection 2 and Collection 3 surface reflectance and NDVI (in terms of magnitude, spatial and spatio-temporal pattern)?
- How do these differences relate to the changes in the processing chain?

6.1.1. SPOT4-VEGETATION1 (VGT1)

6.1.1.1. Product completeness and status map labelling

The differences in product completeness between Collection 2 and 3 are shown in Table 10. It is evident that the amount of clear observations in Collection 3 is significantly less, due to more detected clouds and cloud shadows, while the snow/ice fraction in Collection 3 is slightly less from Collection 2.

Table 10: Overall difference in status map labelling Collection 3 - Collection 2 for VGT1 (% land pixels, April 1998 – January 2003).

Label	Collection 2 VGT1 [%]	Collection 3 VGT1 [%]	Difference [%]
Clear	78.97	72.55	-6.42 %
Not clear	21.03	27.44	
Missing	7.56	7.53	-0.03 %
Cloud/shadow	3.08	10.02	+6.94 %
Snow/ice	10.39	9.89	-0.50 %

6.1.1.2. Spatio-temporal analysis of the differences between C2 and C3

Figure 15 shows Hovmöller plots, i.e., the temporal evolution along a latitudinal gradient, of the systematic difference and the mean bias difference between the reflectances and NDVI from C2 and C3. Both differences are expressed in percentage reflectance. The comparison is based on cloud free observations in the S10 data, with additional sampling for identical day of observation, viewing zenith angle less than 30° and no mixed scatter observations.

An extensive analysis on the differences between Collection 2 and 3 surface reflectance and NDVI revealed the following:

- A sharp edge can be observed in May 2001. This is related to the change in algorithms for cloud, snow/ice labelling and atmospheric correction in Collection 2 (see sections 5.2 and5.5).
- The seasonal pattern in the two difference metrics is related to the correct Sun-Earth distance modelling in the C3 data set. This results in a higher reflectance value during summer and a lower reflectance value during winter in the C3 data set. For NDVI, the impact of the Sun-Earth distance modelling is much less pronounced, especially after May 2001.
- Differences between Collection 2 and Collection 3 are smaller in vegetated areas and larger in bare areas.
- Differences over the years are related to the change in the Atmospheric Correction and a trend, connected to changes in the calibration coefficients, is visible.

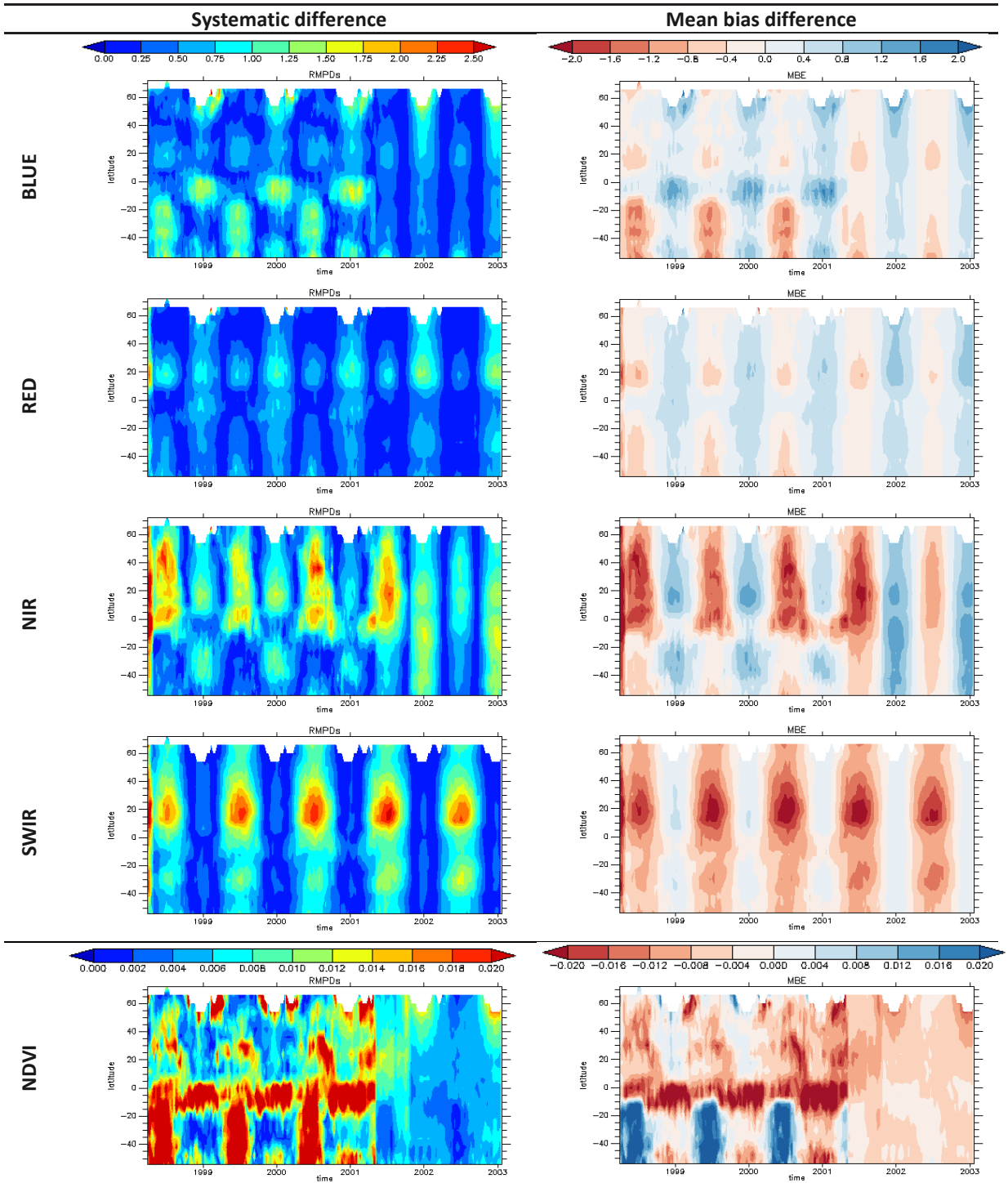

Figure 15: Hovmöller plots of the systematic difference (left) and mean bias difference (right, C2 minus C3) between the reflectances and NDVI from C2 and C3 VGT1

6.1.2. SPOT5-VEGETATION2 (VGT2)

6.1.2.1. Product completeness and status map labelling

Table 11 summarizes the amount of clear/unclear observations over land, for the period February 2003 – May 2014. Collection 3 shows less clear observations, especially related to a larger amount of clouds/shadows detected. Further, less pixels are detected as snow/ice. The amount of missing observations (due to illumination conditions or bad radiometric quality) remains unchanged.

Table 11: Overall difference in status map labelling Collection 3 – Collection 2 for VGT2 (% land pixels, February 2003 – May 2014)

Label	Collection 2 VGT2 [%]	Collection 3 VGT2 [%]	Difference [%]
Clear	76.57 %	71.91 %	-4.66 %
Not clear	23.43 %	28.09 %	
Missing	7.32 %	7.31 %	-0.01 %
Cloud/shadow	4.86 %	11.02 %	+6.16 %
Snow/ice	11.24 %	9.75 %	-1.49 %

The temporal evolution of land pixels with clear observations or flagged as missing, cloud/shadow or snow/ice revealed a similar pattern over the years.

6.1.2.2. Spatio-temporal analysis of the differences between C2 and C3

Figure 16 shows Hovmöller plots, i.e. the temporal evolution along a latitudinal gradient, of the systematic difference and the mean bias difference between the reflectances and NDVI of VGT2 from C2 and C3. Both differences are expressed in percentage reflectance. The comparison is based on cloud free observations in the S10 data, with additional sampling for identical day of observation, viewing zenith angle less than 30° and no mixed scatter observations.

The following patterns can be observed:

- The seasonal trend in the difference between C2 and C3 is related to the correct modelling of the Sun-Earth distance.
- Similar as to VGT1, surface reflectances are generally slightly higher for Collection 3, with the largest differences for the NIR and SWIR channels.

For RED, and consequently also for NDVI, the change in absolute calibration coefficients is clearly expressed in the difference between the C2 and C3 time series (see Figure 13).

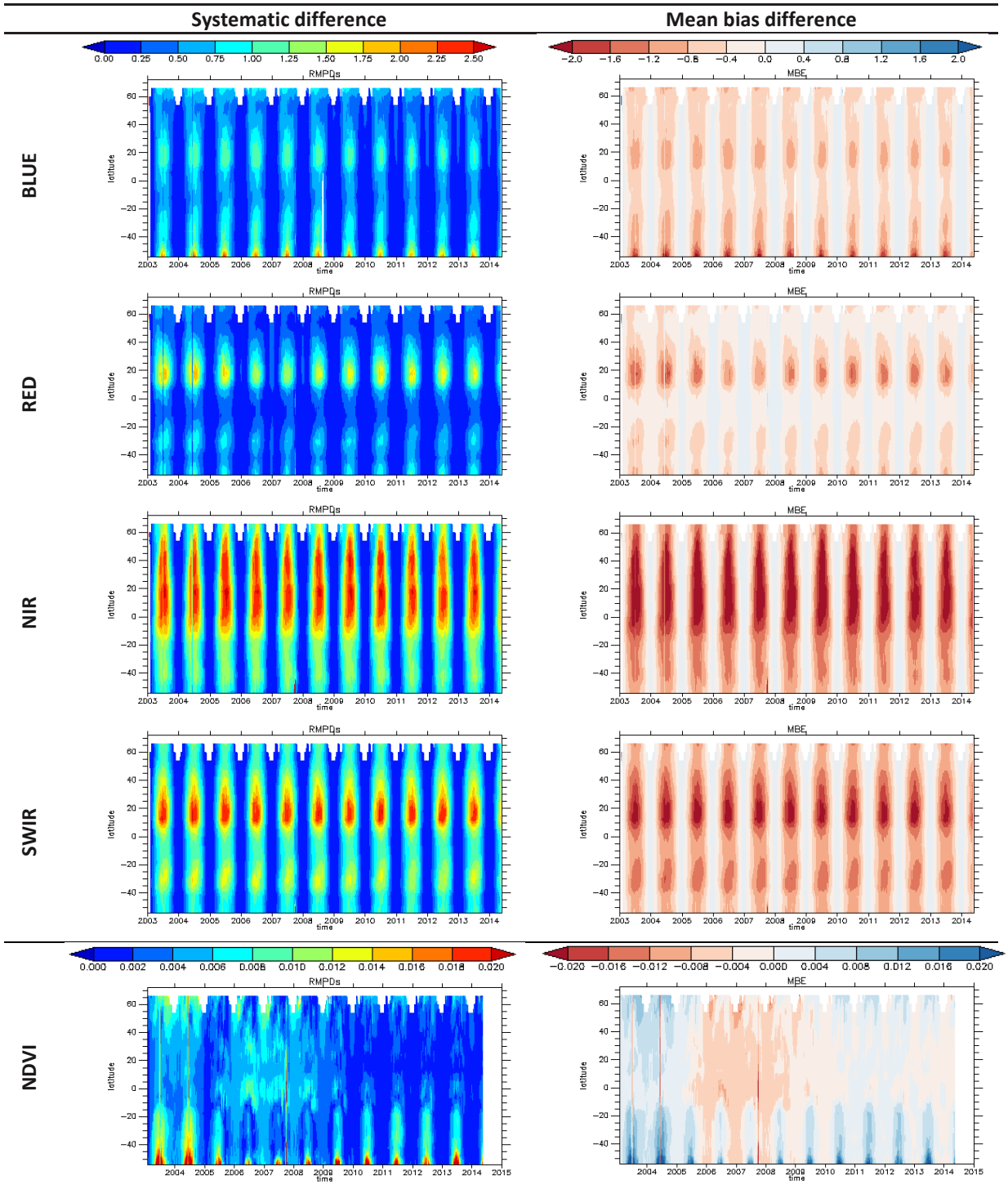

Figure 16: Hovmöller plots of the systematic difference (left) and mean bias difference (right, C2 minus C3) between the reflectances and NDVI from C2 and C3 VGT2.

6.2. Consistency between VGT1 and VGT2

Figure 17 shows the Hovmöller plots, i.e., the temporal evolution along a latitudinal gradient, of the systematic difference and the mean bias difference between the reflectances and NDVI of VGT1 and VGT2 from C3 for the period April/2004 – April/2007. Both differences are expressed in percentage reflectance. Only cloud free observations with viewing zenith angle less than 30° and no mixed scatter observations are used from the S10 composites.

For surface reflectances, there is no spatio-temporal pattern in the bias, except for an outlier in July/2005. This is caused by a number of missing segments for 20050711. The bias is for all spectral bands less than 1% reflectance, except for the extreme high latitude. The faint seasonal pattern in the differences is explained by their small difference in overpass time between SPOT4 and SPOT5.

In contrast, the NDVI shows a larger bias in the tropics and in the Northern hemisphere boreal areas. While in other areas the bias is close to 0, these areas show a positive bias, indicating VGT2 NDVI is higher than VGT1 NDVI for these areas. Overall, the difference between VGT1 and VGT2 is small.

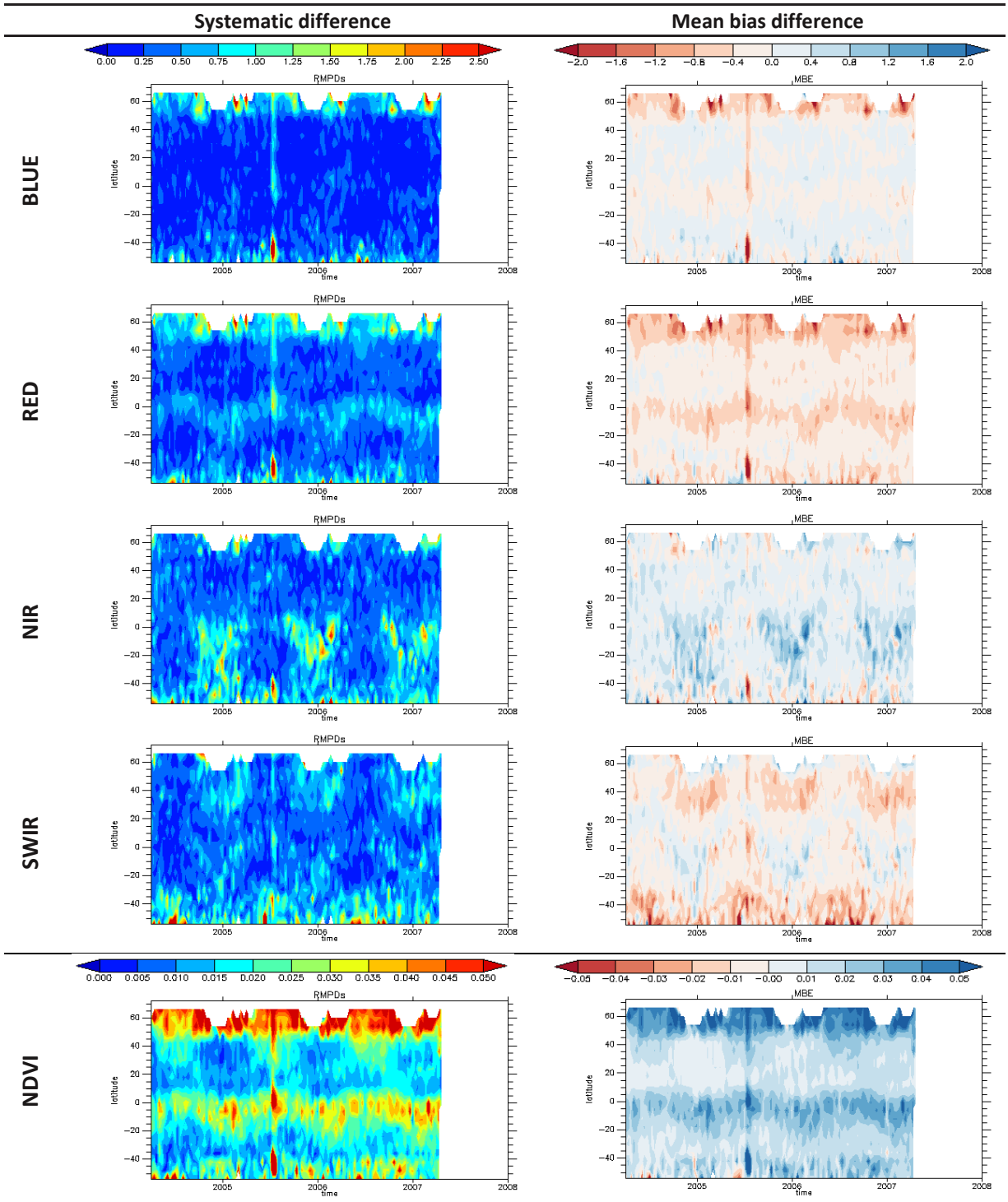

Figure 17: Hovmöller plots of the systematic difference (left) and mean bias difference (right, VGT2 minus VGT1) between the reflectances and NDVI from C3 VGT1 and C3 VGT2

7. Product data access and description

7.1. SPOT-VGT product data access

The SPOT-VGT data available at the VITO Earth Observation (EO) portal can only be accessed upon registration. Figure 18 shows the portal's main page.

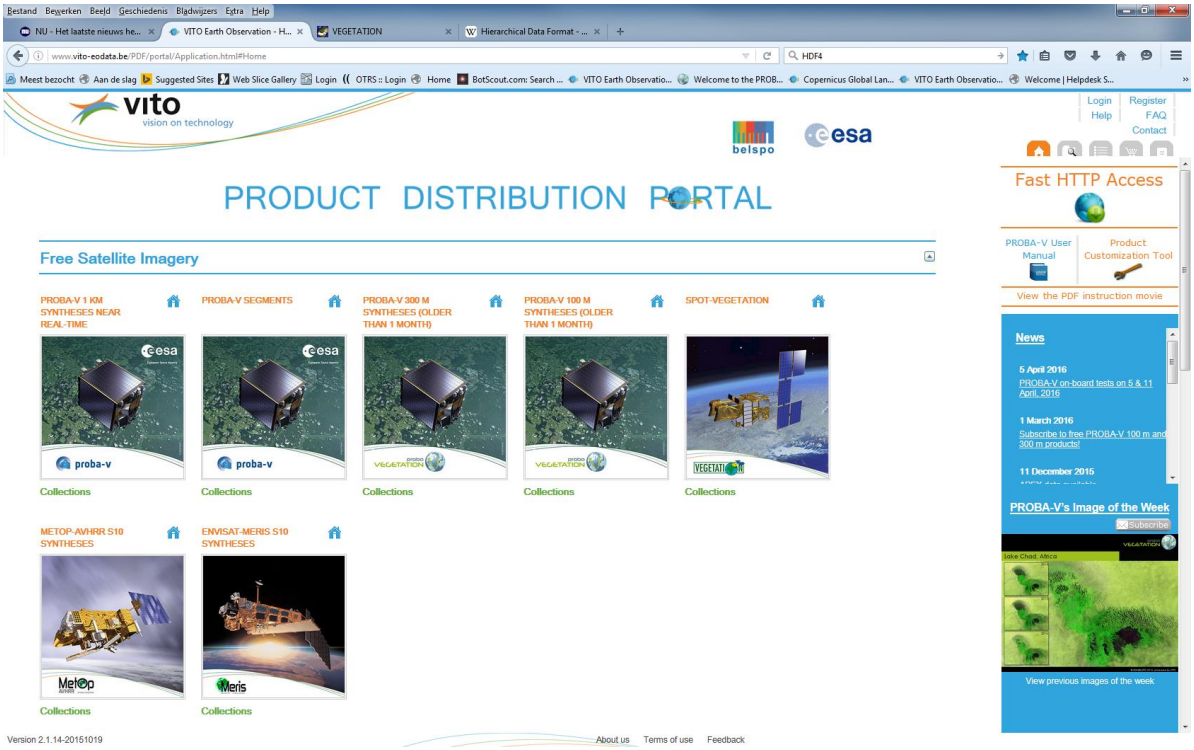

Figure 18: Screen shot of VITO's Earth Observation portal's main page.

Registration can proceed after clicking the 'Register' link in the portal main page's upper-right corner. After clicking the link, a form to be filled out by the user appears on top of the portal's main page, see Figure 19. The user is requested to provide additional information and to accept the Terms and Conditions. After clicking the 'Register' button, an e-mail with an activation link is sent to the user and registration is completed.

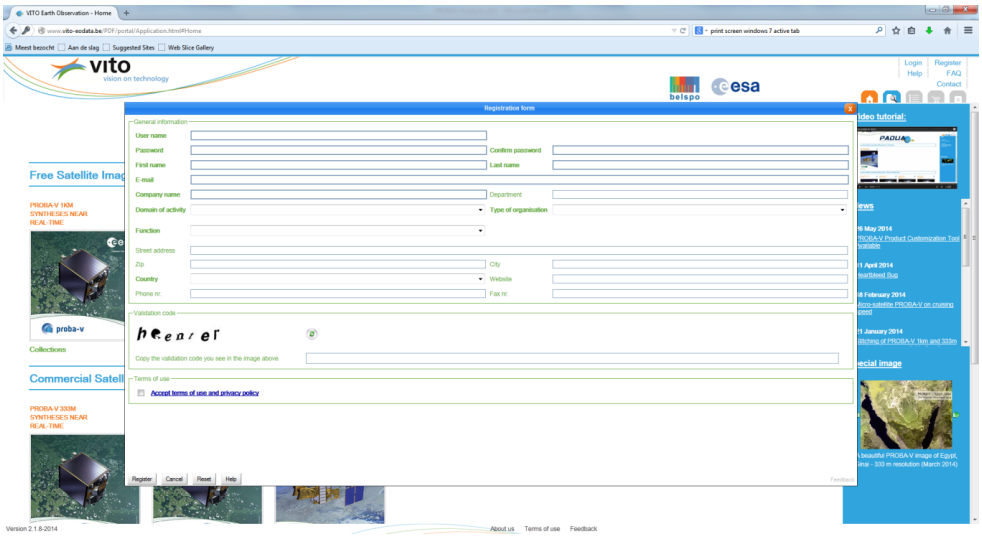

Figure 19: User registration form.

The following SPOT-VGT data products are available from the portal:

- FreeP (Level 2 TOA data)
- S1 products
- S10 NDVI – continental extracts
- S10 Radiometric – continental extracts

After selection of one or more products, the user has the following options:

1. **Back to search:** go back and refine the search
2. **Prepare order:** proceed with the selected product(s). The user can further specify details (e.g. choose the delivery method: FTP pull, FTP push, HTTP download) and refine the dataset selection. Further, an option exists to have multiple product tiles stitched into a single product output file.
3. **Fast order by FTP:** by clicking this button, all selected products are ordered non-customised and delivered via FTP pull. Figure 20 shows an order example ready for submission.

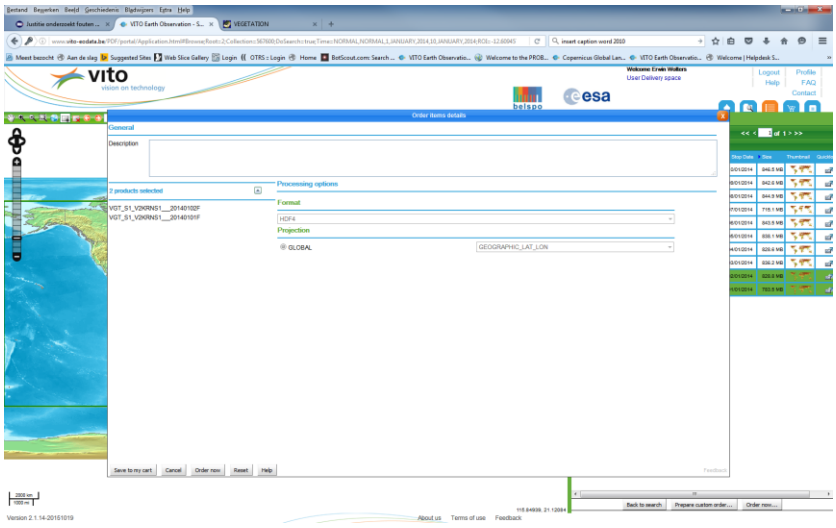

Figure 20: Ordering global S1 files for 1 and 2 January 2014.

In case of registration, search and order problems, as well as other technical and scientific issues the VITO Remote Sensing Helpdesk can be contacted via helpdeskticket@vgt.vito.be.

7.2. Product data description

7.2.1. File naming conventions

SPOT-VGT data are made available from the VITO Earth Observation Portal as zip files. These zip files are located in directories with the following naming structure:

VGT_<*product_id*>_V<*instrument_id*>KRN<*product_id*>__<*yyyymmdd*>F<*segment_id*>V<*version_nr*>, e.g.
VGT_P_V2KRNP____20140125F129V003, with acronym "KRN" referring to the Kiruna receiving station. The <*segment_id*> is only available for the P products.

The filename convention for the Collection 3 P product zip files is as follows:

<*sat*>_<*instrument*>_<*product_id*>_____<*yyyymmddhhmmss_yyyymmddhhss*>_CVB_<*orbit_id*>_V<*version_nr*>.ZIP. For example

SV05_VG2_P_____20140125061522_20140125064131_CVB_83_V003.ZIP

The elements in this filename are explained in Table 12.

Table 12: Explanation of the filename elements.

element	meaning
<sat>	SPOT4 or SPOT5
<instrument>	VGT1 or VGT2
<product_id>	P

<yyyymmddhhmmss_yyyymmddhhss>	beginning and end time of observations for the product
CVB	the Image Processing Centre at VITO
<orbit_id>	orbit number
V<version_nr>	File version number, the reprocessed data have version number 003

For synthesis products, the file naming convention is:

<sat>_<instrument_id>_<product_id>___<product_type>___<yyyymmddhhmmss_yyyymmddhhss> _CVB_*<orbit_id>*_V*<version_nr>*.ZIP

element	**meaning**
<sat>	SPOT5 satellite
<instrument_id>	VGT2 instrument
<product_id>	S1/S10 synthesis
<product_type>	Indicates whether the synthesis contains radiometry (RM) or NDVI data (NDVI)
<yyyymmddhhmmss_yyyymmddhhss>	beginning and end time of observations for the product
CVB	the Image Processing Centre at VITO
<orbit_id>	orbit number, default value '000000'
<continent>	The continent name, only available for the continental extracts
V*<version_nr>*	File version number, the reprocessed data have version number 003

Synthesis data are also available for 9 predefined continental areas:

- Africa
- Australasia
- N-Asia
- SE-Asia
- W-Asia
- Asian Islands
- N-America
- Central America
- S-America
- Europe

7.2.2. VGT P-products

Table 13 shows the contents of the SPOT-VGT P product. After extracting the zip file, the user will see a directory of the form V2*<yyyymmddxxx>,* with suffix *<xxx>* referring to the SPOT-VGT segment number. Inside this directory, the following files are stored (see Table 13).

Table 13: Contents of SPOT-VGT P-product.

Dataset	Content
V2<yyyymmddxxx>_1BL.HDF	Latitude collocation data with SPOT-HRVIR
V2<yyyymmddxxx>_1BO.HDF	Longitude collocation data with SPOT-HRVIR
V2<yyyymmddxxx>_AG.HDF	aerosol grid
V2<yyyymmddxxx>_B0.HDF	B0 spectral reflectances
V2<yyyymmddxxx>_B2.HDF	B2 spectral reflectances
V2<yyyymmddxxx>_B3.HDF	B3 spectral reflectances
V2<yyyymmddxxx>_LOG.TXT	Logical Volume Descriptor
V2<yyyymmddxxx>_MIR.HDF	MIR spectral reflectances
V2<yyyymmddxxx>_OG.HDF	Ozone grid
V2<yyyymmddxxx>_QL.TIF	Quicklook image based on the B2 channel
V2<yyyymmddxxx>_RIG.TXT	Copyright text file
V2<yyyymmddxxx>_SAA.HDF	Solar Azimuth Angles
V2<yyyymmddxxx>_SM.HDF	Status Map information
V2<yyyymmddxxx>_SZA.HDF	Solar Zenith Angles
V2<yyyymmddxxx>_VAA.HDF	Viewing Azimuth Angles
V2<yyyymmddxxx>_VZA.HDF	Viewing Zenith Angles
V2<yyyymmddxxx>_WVG.HDF	Water Vapour Grid

Further, each data layer is accompanied by one or more HDF4 attribute tables, which give information on the number of lines and columns, the datatype, bit lengths, calibration coefficients where applicable, etc. Detailed attribute table descriptions can be found in Appendix 1.

The Logical Volume Descriptor file contains the following information:

- The product (spectral band or auxiliary data reference)
- Projection information (type, unit, geodetic parameters, resolution, etc.)
- Geotie points (upper left, lower left, upper right, and lower right coordinates)
- Reference to geometric correction PCI file
- Reference to radiometric correction PCI file
- Segment start and end date
- Cloud and snow/ice detection algorithm version
- Production date

7.2.3. S1 product

After extracting the S1 zip file, a directory with name *<nr>.<yyyymmdd>*S1 appears, with *<nr>* being '1' for VGT1 and '2' for VGT2, and *<yyyymmdd>* referring to the synthesis date. The contents of this directory are shown in Table 14.

Table 14: Contents of the S1 product.

Dataset	Content
*<nr>.<yyyymmdd>*_B0.HDF	B0 spectral reflectances
*<nr>.<yyyymmdd>*_B2.HDF	B2 spectral reflectances
*<nr>.<yyyymmdd>*_B3.HDF	B3 spectral reflectances
*<nr>.<yyyymmdd>*_LOG.TXT	Logical Volume Descriptor

<nr>.<yyyymmdd>_MIR.HDF	MIR spectral reflectances
<nr>.<yyyymmdd>_NDV.HDF	NDVI
<nr>.<yyyymmdd>_QL.TIF	Quicklook image
<nr>.<yyyymmdd>_RIG.TXT	Copyright text file
<nr>.<yyyymmdd>_SAA.HDF	Solar Azimuth Angles
<nr>.<yyyymmdd>_SM.HDF	Status Map information
<nr>.<yyyymmdd>_SZA.HDF	Solar Zenith Angles
<nr>.<yyyymmdd>_TG.HDF	Time Grid
<nr>.<yyyymmdd>_VAA.HDF	Viewing Azimuth Angles
<nr>.<yyyymmdd>_VZA.HDF	Viewing Zenith Angles

7.2.4. S10 product

After extracting the S10 zip file, a directory with name *<nr>.<yyyymmdd>*S10 appears, with *<nr>* being '1' for VGT1 and '2' for VGT2 and *<yyyymmdd>* referring to the starting date of the 10-day synthesis.

Table 15: Contents of the S10 product

Dataset	Content
<nr>.<yyyymmdd>_B0.HDF	B0 spectral reflectances
<nr>.<yyyymmdd>_B2.HDF	B2 spectral reflectances
<nr>.<yyyymmdd>_B3.HDF	B3 spectral reflectances
<nr>.<yyyymmdd>_LOG.TXT	Logical Volume Descriptor
<nr>.<yyyymmdd>_LOG.TXT	Logical Volume Descriptor
<nr>.<yyyymmdd>_MIR.HDF	MIR spectral reflectances
<nr>.<yyyymmdd>_NDV.HDF	NDVI dataset
<nr>.<yyyymmdd>_QL.TIF	Quicklook image
<nr>.<yyyymmdd>_RIG.TXT	Copyright text file
<nr>.<yyyymmdd>_SAA.HDF	Solar Azimuth Angles
<nr>.<yyyymmdd>_SM.HDF	Status Map
<nr>.<yyyymmdd>_SZA.HDF	Solar Zenith Angles
<nr>.<yyyymmdd>_TG.HDF	Time Grid
<nr>.<yyyymmdd>_VAA.HDF	Viewing Azimuth Angles
<nr>.<yyyymmdd>_VZA.HDF	Viewing Zenith Angles

7.3. Conversion factors, status map, and geolocation

7.3.1. Conversion factors

The conversion of SPOT-VGT image pixel values (DN) to physical values (PV) is done via:

$$PV = a * \mathrm{DN} + b$$

For reflectance values, the values for *a* and *b* are 0.0005 and 0, respectively, while for the NDVI product these values are 0.004 and -0.1. This gives a physical NDVI range of [-0.1, 0.92].

7.3.2. Status Map

In the SPOT-VGT P, S1 and S10 files, the Status Map contains a quality state indicator for each pixel, consisting of an observation indicator (clear, cloud, ice, shadow, undefined), a land/sea flag, and a radiometric quality indicator. Table 16 explains the Status Map pixel quality indicators.

Table 16: Explanation of the pixel quality indicators in the Status Map.

Bit (LSB to MSB)	Description	Value	Key
0-2	Cloud/Ice Snow/Shadow Flag	000 001 010 011 100	Clear Shadow Undefined Cloud Ice
3	Land/Sea	0 1	Sea Land
4	Radiometric quality SWIR flag	0 1	Bad Good
5	Radiometric quality NIR flag	0 1	Bad Good
6	Radiometric quality RED flag	0 1	Bad Good
7	Radiometric quality BLUE flag	0 1	Bad Good

7.3.3. Geolocation information

The SPOT-VGT data are available in Plate Carreé (WGS84) projection at the nominal 1 km (or 1/112°) resolution. The pixel geolocation is provided for the pixel centre, which means that the latitudinal and longitudinal pixel extent is [*lon*-1/224°:*lon*+1/224°, *lat*-1/224°:*lat*+1/224°], see Figure 21.

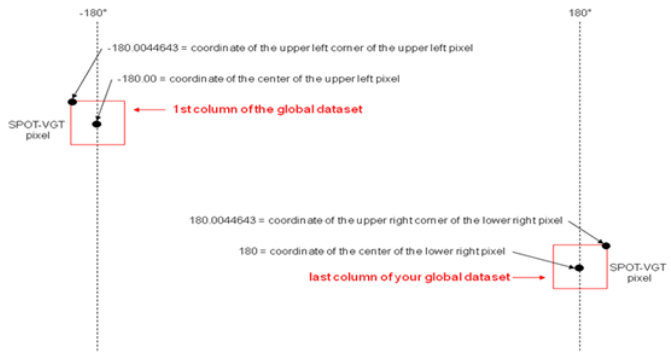

Figure 21: SPOT-VGT image coordinate definition.

REFERENCES

Ackerman, S., K. Strabala, W.P. Menzel, R. Frey, C. Moeller, and L. Gumley (2010), Discriminating clear-sky from cloud with MODIS: Algorithm Theoretical Basis Document (MOD35) version 6, *MODIS Cloud Mask Team, Cooperative Institute for Meteorological Satellite Studies (CIMSS), University of Wisconsin*.

Bartalev S.A., V. A. Egorov, E. A. Loupian, and I. A. Uvarov, (2007), Multi-year circumpolar assessment of the area burnt in boreal ecosystems using SPOT-VEGETATION, *Int. J. Remote Sens.*, *28*, 1397 – 1404.

Berry, P. A. M., R.A. Pinnock, R.D. Hilton, and C.P.D. Johnson, (2000), ACE: A new global digital elevation model incorporating satellite altimeter derived heights. *European Space Agency, ERS-ENVISAT Symposium, Gothenburg, Sweden, Oct. 2000.*

Berthelot, B., and G. Dedieu, (1997), Correction of atmospheric effects for VEGETATION data, *Physical Measurements and Signatures in Remote Sensing, Courchevel, France*, 19 – 25.

Berthelot, B., (2004), Snow detection on VEGETATION data - Improvement of cloud screening (No. NOV-3128-NT-2295, v1.1), 54 pp.

Boschetti, M. , F. Nutinia, P.A. Brivio, E. Bartholome, D. Stroppiana, and A. Hoscilo, (2013), Identification of environmental anomaly hot spots in West Africa from time series of NDVI and rainfall, *ISPRS J. Photogramm.*, *78*, 26 – 40.

Bouvet, M., (2014), Radiometric comparison of multispectral imagers over a pseudo-invariant calibration site using a reference radiometric model. *Remote Sens. Environ.*, *140*, 141 – 154.

Danko, D. M. (1992). The digital chart of the world project. *Photogramm. Eng. Rem. S.*, *58*, 1125 – 1128.

Doelling, D. R., D. Morstad, B. R. Scarino, R. Bhatt, and A. Gopalan, A. (2013), The characterization of deep convective clouds as an invariant calibration target and as a visible calibration technique. *Geoscience and Remote Sensing, IEEE T. Geosci. Remote*, *51*, 1147 – 1159.

Eva H.D., A.S. Belward, E.E. De Miranda, C.M. Di Bella, V. Gond, O. Huber, S. Jones, M. Sgrenzaroli, and S. Fritz, (2004), A land cover map of South America, *Glob. Change Biol., 10*, 731-744.

Fernandes, J.L., J.V. Rocha, and R.A.C. Lamparelli, (2011), Sugarcane yield estimates using time series analysis of spot vegetation images, *Sci. Agr.*, *68*, 139-146.

Garrigues, S., et al. (2008), Validation and intercomparison of global Leaf Area Index products derived from remote sensing data, *J. Geophys. Res.-Biogeo,* 113*, G02028,* doi:10.1029/2007JG000635.

Hagolle, O., J.M. Nicolas, B. Fougnie, F. Cabot, and P. Henry (2004). Absolute calibration of VEGETATION derived from an interband method based on the sun glint over ocean, *IEEE T. Geosci. Remote, 42*, 1472 – 1481.
Henry P. and A. Meygret, (2001), Calibration of VEGETATION cameras onboard SPOT4. *Proceedings of the VEGETATION 2000 conference, Belgirate- Italy, 3-6 April 2000 , Saint G. (Ed), CNES - Toulouse & JRC - Ispra*, 23 – 32.

Ivits, E., M. Cherlet, T. Toth, K. E. Lewiska, and G. Toth, (2011), Characterisation of productivity limitation of salt-affected lands in different climatic regions of Europe using remote sensing derived productivity indicators, *Land Degr. Dev.*, *24*, 438 – 452.

Lachérade, S., B. Fougnie, P. Henry, P. Gamet, and P. Cross, (2013), Calibration Over Desert Sites: Description, Methodology, and Operational Implementation. *IEEE Transact. Geosci. Remote*, *51*, 1098 – 1113.

Latifovic R., Zhi-Liang Zhu, Josef Cihlar, Chandra Giri, Ian Olthof, 2004, Land cover mapping of North and Central America - Global Land Cover 2000, *Remote Sens. Environ., 89*, 116-127.

Lissens, G., Kempeneers, P., Fierens, F., and Van Rensbergen, J. (2000). Development of cloud, snow, and shadow masking algorithms for VEGETATION imagery. In *Geoscience and Remote Sensing Symposium, 2000. Proceedings. IGARSS 2000. IEEE 2000 International* (Vol. 2, pp. 834-836). IEEE.

Maisongrande P., B. Duchemin, B. Berthelot, C. Dubegny, G. Dedieu, and M. Leroy (2001), A new algorithm concept for atmospheric correction of surface reflectances delivered by the VEGETATION system. *Proceedings of the VEGETATION 2000 conference, Belgirate, Italy, 3 – 6 April 200, Saint G. (Ed), CNES - Toulouse & JRC - Ispra*, 307 – 312.

Maisongrande P., B. Duchemin, and G. Dedieu, (2004), VEGETATION/SPOT: an operational mission for Earth monitoring: Presentation of new standard products, *Int. J. Remote Sens.*, 9 – 14.

Mayaux P., P. Holmgren, F. Achard, H. Eva, H.-J. Stibig, and A. Branthomme, (2005), Tropical forest cover change in the 1990s and options for future monitoring, *Philos. T. Roy. Soc. B.*, *360*, 373 – 384.

Pacholczyk, P, Makhmara, H and Lacaze, R, 2012, 12 years time series of SPOT / VEGETATION biophysical variables, *EGU General Assembly Conference Abstracts*, *Vol. 14*, p. 9368).

Quang, C, 2015, Analyse des defauts d'égalisation haute des defauts dégalisation haute frequencies des instruments Vegetation, *CNES-CS*, 88 pp.

Quesney, A. (2008), A multi-sensor generic cloud screening toolbox, *CYCLOPES project document NOV-3128-NT-1759*, 38 pp.

Rahman, H., and G. Dedieu, G. (1994), SMAC: a simplified method for the atmospheric correction of satellite measurements in the solar spectrum. Int. J. *Remote Sens.*, *15*, 123 – 143.

Rojas O., F. Rembold, A. Royer, and T. Negre, (2005), Real-time agrometeorological crop yield monitoring in Eastern Africa., *Agron. Sustain. Dev., 25,* 63 – 77.

Savin Y.I., D. Stathakis, T. Negre and V. A. Isaev, (2007), Prediction of crop yields with the use of neural networks, *Russian Agricultural Sciences*, 33, 361 – 363.

Simpson, J.J., Z. Jin, and J.R. Stitt (2000), Cloud shadow detection under arbitrary viewing and illumination conditions, *IEEE Transact. Geosci. Remote, 38,* 972 – 976.

Sohn, B. J., S.H. Ham, and P. Yang, (2009), Possibility of the visible-channel calibration using deep convective clouds overshooting the TTL. *J. Appl. Meteorol. Clim.*, *48*, 2271 – 2283.

Sterckx, S., S. Livens, and S. Adriaensen, (2013), Rayleigh, deep convective clouds, and cross-sensor desert vicarious calibration validation for the PROBA-V mission., *IEEE Transact. Geosci. Remote, 51*(3), 1437 – 1452.

Sterckx, S., et al. (2014), The PROBA-V mission: image processing and calibration. *Int. J. Remote Sens.*, *35*, 2565 – 2588.

Stibig H-J., A.S. Belward, P.S. Roy, U. Rosalina-Wasrin, S. Agrawal, P.K. Joshi, Hildanus, R. Beuchle, S. Fritz, S. Mubareka and C. Giri, 2007, A land-cover map for South and Southeast Asia derived from SPOT-VEGETATION data, *J. Biogeogr.*, *34*, 625 – 637.

Sylvander, S., I. Albert-Grousset, and P. Henry, (2003), Geometrical performance of the VEGETATION products, in: *Geoscience and Remote Sensing Symposium, 2003. IGARSS'03. Proceedings. 2003 IEEE International* (Vol. 1, 573 – 575).

Tansey K., et al. (2004), Vegetation burning in the year 2000: Global burned area estimates from SPOT VEGETATION data, *J. Geophys. Res-Atmos., 109*, 2156 – 2202, doi:10.1029/2003JD003598.

Tanre, D., J.L. Deuze, M. Herman, R. Santer, and E. Vermote, E. (1990), Second simulation of the satellite signal in the solar spectrum-6S code, In: *Geoscience and Remote Sensing Symposium, 1990. IGARSS'90.'Remote Sensing Science for the Nineties'., 10th Annual International* (187 – 187).

Toté, C., E. Swinnen, and S. Sterckx, (2016), Evaluation of the re-processed VGT1 and VGT2 archive, *VITO Scientific Report*, 60 pp.

Verdin J., C. Funk, G. Senay, R. Choularton, (2005), Climate science and famine early warning, *Philos. T. Roy. Soc. B.*, *360*, 2155 – 2168.

Verger A., F. Camacho, F.J. Garcia-Haro, J. Melia, 2009, Prototyping of Land-SAF leaf area index algorithm with VEGETATION and MODIS data over Europe, *Remote Sens. Environ.*, *113*, 2285-2297.

Vermote, E., and Y.J. Kaufman, (1995), Absolute calibration of AVHRR visible and near-infrared channels using ocean and cloud views. *Int. J. Remote Sens.*, *16*, 2317 – 2340.

Vermote, E., R. Santer, P.Y. Deschamps, and M. Herman, (1992), In-flight calibration of large field of view sensors at short wavelengths using Rayleigh scattering. *Int. J. Remote Sens.*, *13*, 3409 – 3429.

Zhang Q., G. Pavlic, W. Chen, R. Latifovic, R. Fraser, J. Cihlar, (2004), Deriving stand age distribution in boreal forests using SPOT-VEGETATION and NOAA-AVHRR imagery, *Remote Sens. Environ., 91*, 405 – 418.

Zhu, Z., and C.E. Woodcock, (2012), Object-based cloud and cloud shadow detection in Landsat imagery. *Remote Sens. Environ.*, *118*, 83 – 94.

APPENDICES

Appendix 1: Attribute Tables

Each HDF4 dataset is accompanied by an attribute table, which provides additional information to the user on data size, calibration and conversion factors, as well as the spectral TOA solar irradiance for the reflectance datasets. The Table below shows all Attribute Fields, with the first row containing the generic fields.

Dataset (filename suffix)	Attribute Tables	Attribute Fields	Product type
All	All	NUMBER_OF_LINES NUMBER_OF_PIXELS NUMBER_OF_BITS	All
HRVIR Collocation (BL, BO)	1B HRVIR LATITUDE PLANE1B HRVIR LONGITUDE PLANE1B	PIXEL_NUMBER_REF_LOC LINE_NUMBER_REF_LOC 1BHRVIR_LAT_COEF_A 1BHRVIR_LAT_COEF_B	P
Reflectance datasets (B0, B1, B3, MIR)	SPECTRAL BAND B0/2/3/MIR	ABS_CALIB_COEF ANALOG_GAIN ON_BOARD_GAIN NORMAL_SOLAR_IRR COEF_A OFFSET_B	P, S1, S10
Auxiliary datasets (AG, OG, WVG)	AEROSOL GRID OZONE GRID WATER VAPOUR GRID	PIXEL_SAMPLING LINE_SAMPLING PIXEL_NUMBER_REF_LOC LINE_NUMBER_REF_LOC	P
Status Map	STATUS MAP	PERCENT_LAND PERCENT_CLOUD PERCENT_SNOW_ICE	P, S1, S10
Angular datasets	SOLAR ZENITH ANGLE VIEWING AZIMUTH ANGLE VIEWING ZENITH ANGLE	PIXEL_SAMPLING LINE_SAMPLING PIXEL_NUMBER_LOC_REF LINE_NUMBER_LOC_REF	P, S1, S10
NDVI	NDVI	NDVI_COEF_A NDVI_OFFSET_B	S1, S10
Time Grid	TG	SYNTH_REF_DATE SYNTH_REF_TIME	S1, S10

Appendix 2: Known missing SPOT-VGT Collection 3 data

Although several major issues have been addressed during the reprocessing campaign, some minor issues were discovered due to payload, archiving, and missing data issues. The tables below summarize these issues.

Data missing due to payload issues

Sensor	Date start	Date end	Comment	Impact on
VGT2	22/02/2012	23/02/2012	No programming on-board due to power constraints	P, S1, S10
VGT2	07/03/2008	11/03/2008	Technical problems on the VGT2 payload	P, S1, S10
VGT2	06/09/2007	12/09/2007	Technical problems on the VGT2 payload	P, S1, S10

Data missing due to archiving issues

Sensor	Date start	Date end	Comment	Impact on
VGT2	27/08/2007	27/08/2007	Segment 178 missing, could not be retrieved	P
VGT2	30/01/2004	30/01/2004	Segment 234 missing, could not be retrieved	P
VGT2	22/01/2004	22/01/2004	Segment 231 missing, could not be retrieved	P
VGT2	22/01/2004	22/01/2004	Segment 221 missing, could not be retrieved	P
VGT1	21/04/2000	21/04/2000	Segment 245 missing, could not be retrieved	P
VGT1	28/12/1999	28/12/1999	Segment 241 missing, could not be retrieved	P
VGT1	19/06/1998	19/06/1998	Segment 050 missing, could not be retrieved	P
VGT1	16/05/1998	16/05/1998	Segment 029 missing, could not be retrieved	P

Data missing

Sensor	Date start	Date end	Comment	Impact on
VGT1	11/08/1999	11/08/1999	Segment 247 not used due to solar eclipse	S1, S10
VGT2	29/03/2006	29/03/2006	Segments 047 and 049 not used due to solar eclipse	S1, S10
VGT2	03/10/2005	03/10/2005	Segments 126 and 127 not used due to solar eclipse	S1, S10